

# Human-like conceptual representations emerge from language prediction

Ningyu Xu<sup>1,2</sup>, Qi Zhang<sup>1,3</sup>, Chao Du<sup>4</sup>, Qiang Luo<sup>4</sup>,  
Xipeng Qiu<sup>1\*</sup>, Xuanjing Huang<sup>1,5\*</sup>, Menghan Zhang<sup>2,4,6\*</sup>

<sup>1</sup>School of Computer Science, Fudan University, Shanghai, China.

<sup>2</sup>Institute of Modern Languages and Linguistics, Fudan University,  
Shanghai, China.

<sup>3</sup>Shanghai Key Laboratory of Intelligent Information Processing, Shanghai,  
China.

<sup>4</sup>Research Institute of Intelligent Complex Systems, Fudan University,  
Shanghai, China.

<sup>5</sup>Shanghai Collaborative Innovation Center of Intelligent Visual  
Computing, Shanghai, China.

<sup>6</sup>Ministry of Education Key Laboratory of Contemporary Anthropology,  
Fudan University, Shanghai, China.

\*Corresponding author(s). E-mail(s): [xpqi@fudan.edu.cn](mailto:xpqi@fudan.edu.cn);  
[xjhuang@fudan.edu.cn](mailto:xjhuang@fudan.edu.cn); [mhzh@fudan.edu.cn](mailto:mhzh@fudan.edu.cn);

## Abstract

People acquire concepts through rich physical and social experiences and use them to understand the world. In contrast, large language models (LLMs), trained exclusively through next-token prediction over language data, exhibit remarkably human-like behaviors. Are these models developing concepts akin to humans, and if so, how are such concepts represented and organized? To address these questions, we reframed the classic reverse dictionary task to simulate human concept inference in context and investigated the emergence of human-like conceptual representations within LLMs. Our results demonstrate that LLMs can flexibly derive concepts from linguistic descriptions in relation to contextual cues about other concepts. The derived representations converged towards a shared, context-independent structure that effectively predicted human behavior across key psychological phenomena, including computation of similarities, categories and semantic scales. Moreover, these representations aligned well with neural activity patterns in the human brain, even in response to visual rather than linguistic stimuli, providing evidence for biological plausibility. These findings establish that structured, human-like conceptual representations can naturally emerge from language prediction without real-world grounding. More broadly, our work positions LLMs as promising computational tools for understanding complex human cognition and paves the way for better alignment between artificial and human intelligence.

## 1 Introduction

Humans are able to construct mental models of the world and use them to understand and navigate their environment [1, 2]. Central to this ability is the capacity to form broad concepts that constitute the building blocks of these models [3]. These concepts, often regarded as mental representations, capture regularities in the world while abstracting away extraneous details, enabling flexible generalization to novel situations [4]. For example, the concept of SUN can be instantly formed and deployed across diverse contexts: observing it rise or set in the sky, yearning for its warmth on a chilly winter day, or encountering someone who exudes positivity. Its role in the solar system can be analogized to the nucleus in an atom, enriching learning and understanding. The nature of concepts has long been a focus of inquiry across philosophy, cognitive science, neuroscience, and linguistics [5–12]. These investigations have uncovered diverse properties that concepts need to satisfy, often framed by the long-standing divide between symbolism and connectionism. Symbolism emphasizes discrete, explicit symbols with structured and compositional properties, enabling abstract reasoning and recombination of ideas [13, 14]. In contrast, connectionism conceptualizes concepts as distributed, emergent patterns across networks, prioritizing continuity and gradedness, which excel in handling noisy inputs and learning from experience [15, 16]. Although there is growing consensus on the need to integrate the strengths of both paradigms to account for the complexity and richness of human concepts [17, 18], reconciling the competing demands remains a significant challenge.

Recent advances in large language models (LLMs) within artificial intelligence (AI) have exhibited human-like behavior across various cognitive and linguistic tasks, from language generation [19, 20] to decision-making [21] and reasoning [22–24]. It has sparked intense interest and debate about whether these models are approaching human-like cognitive capacities based on concepts [25–30]. Some argue that LLMs, trained exclusively on text data for next-token prediction, operate only on statistical associations between linguistic forms and lack concept-based understanding grounded in physical and social situations [29, 31, 32]. This argument is evidenced by their inconsistent performance, which often reveals vulnerabilities such as non-human-like errors and over-sensitivity to minor contextual variations [21, 33, 34]. Conversely, others contend that the performance of a system alone is insufficient to characterize its underlying competence [35], and the extent to which concepts should be grounded remains open [36, 37]. Instead, language may provide essential cues for people’s use of concepts and enable LLMs to approximate fundamental aspects of human cognition, where meaning arises from the relationships among concepts [38, 39]. Despite the conflicting views, there is broad consensus on the central role of concepts in human cognition. The core questions driving the debates are whether LLMs possess human-like conceptual representations and organization and, consequently, whether they can illuminate the nature of human concepts.

To address these questions, we investigated the emergence of human-like conceptual representations from language prediction in LLMs. Our approach unfolded in three stages. First, we examined LLMs’ capacities to derive conceptual representations, focusing on the definitional and structured properties of human concepts. We leveraged LLMs’ in-context learning ability and guided them to infer concepts from descriptions with a few contextual demonstrations (Fig. 1). The models’ outputs offered a behavioral lens to evaluate the derived representations. We explored the organization of these representations by analyzing how their relational structures varied across different contextual demonstrations. Second, we assessed how well the LLM-derived representational structures align with psychological measures and investigated whether they capture rich, context-dependent human knowledge. These questions were tested by leveraging computations over the representations to predict human behavioral judgments. Finally, we mapped the LLM-derived conceptual representations to neural activity patterns in the human brain and analyzed their biological plausibility. Our experiments spanned thousands of naturalistic object concepts and beyond [40], providing a comprehensive analysis of LLMs’ conceptual representations. The findings reveal that language prediction can give rise to human-like conceptual representations and organization in LLMs. These representations integrated many valued aspects of previous accounts, combining the definitional and structural focus of symbolism with the continuity and graded nature of connectionist models. This work underscores the profound connection between language and human conceptual structures and demonstrates that LLM-derived conceptual representations offer a promising foundation for understanding human concepts.

## 2 Results

### 2.1 Reverse dictionary as a conceptual probe

We reframed the reverse dictionary task as a domain-general approach to probe LLMs’ capacity for concept inference. A reverse dictionary identifies words based on provided definitions or descriptions [41], which is simple yet relevant to concept understanding and usage. For instance, consider a child learning that the concept MOON corresponds to both “a round, glowing object that hangs up in the sky at night” and “Earth’s natural satellite”. The child then uses the term “moon”, rather than “circle” or “star”, to refer to this concept. The shared term “moon” helps interlocutors gauge alignment in their understanding of the concept. Instead of relying on a single, potentially ambiguous word (e.g., “bat”), the word-retrieval paradigm combines the words in descriptions to construct coherent meaning, inferring the corresponding concepts and mapping them back to words. The “form-meaning-form” process offers a targeted probe into the models’ capacity to contextually form meaningful representations and appropriately refer to them in ways that align with human understanding.

To guide LLMs through the process, we took advantage of their in-context learning ability and presented them with a small number of demonstrations in a reverse-dictionary format (“[Description]  $\Rightarrow$  [Word]”), followed by a query description (Fig. 1). We then compared model-generated completions to the intended term of the concept corresponding to the query description, thereby evaluating how well the models derived conceptual representations that aligned with human understanding. Formally, given  $N$  pairs of descriptions and words as contextual demonstrations, an LLM  $\mathcal{M}$  encodes the query description of a concept  $c$  into a representation  $\mathbf{h}_c = \text{encode}_{\mathcal{M}}(\text{description} \mid \text{context}_N)$ , and generates a term based on it:  $\text{predict}_{\mathcal{M}}(\mathbf{h}_c)$ . The term was then compared to the name of the query concept shared by humans:  $\text{name}_{\mathcal{H}}(c)$ . We took  $\mathbf{h}_c$  as the representation for concept  $c$ , which immediately precedes the following term that should be in semantic correspondence to the query description. Importantly, the demonstrations provided minimal and controllable context, and the query description served as a special case of general input for concept inference. We can analyze how models construct conceptual representations in response to different contextual cues by varying the number of demonstrations and the specific description-word pairings within them.

### 2.2 Deriving concepts from definitional descriptions

We investigated whether LLMs can construct concepts from definitional descriptions through the reverse dictionary task. Leveraging data from the THINGS database [42], we prompted LLMs with randomly selected description-word pair demonstrations and examined their capacity to predict appropriate terms for the query descriptions (Methods 4.2). Fig. 2 shows the performance of LLaMA3-70B, a state-of-the-art open-source LLM, averaged across five independent runs at varying numbers of demonstrations. The exact match accuracy improved progressively as the number of demonstrations increased from 1 to 24, rising from 79.51% ( $\pm 0.30\%$ ) to 89.45% ( $\pm 0.30\%$ ). Gains were marginal beyond this threshold. These results indicate that, with a few demonstrations

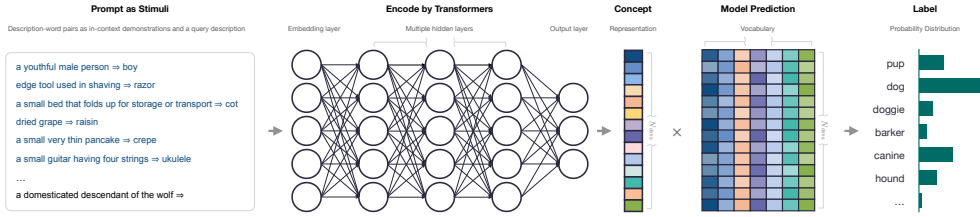


**Fig. 1** Illustration of the reverse dictionary task as a conceptual probe. A Transformer-based LLM is presented with  $N$  description-word pairs as demonstrations in context, followed by a query description. The model is then prompted to encode the query description into a conceptual representation and predict the term that best matches the described concept.

as context, LLMs can effectively combine words into coherent representations and reliably infer the corresponding concepts, despite varying contextual cues.

As a follow-up, we conducted a counterfactual analysis to investigate how LLMs accomplish this: Do they merely function as lookup tables, rigidly mapping descriptions to words, or do they contextually infer concepts based on their interrelationships? As shown in Fig. 2, when presented with only a single demonstration identical to the query description, the model replicated the context, even though the description was paired with a proxy symbol instead of the correct term. As additional correct demonstrations of other concepts were introduced, the model gradually shifted from replication to predicting the proper word for the query concept. This behavior persisted across various proxy symbols, suggesting that contextual cues about other concepts successfully guided the model in disregarding misleading information. When the correct demonstration for the query concept was provided, model performance slightly declined as more demonstrations were added, eventually dropping below the average in the standard generalization setting. This decline indicated that subtle conflicts among demonstrations could arise, with the influence of other concepts overshadowing that of the identical query concept. Collectively, these findings underscore the intricate interrelationships among concepts and their pivotal role in shaping model inference.

Furthermore, we extended our analyses to a broader range of descriptions and concepts to assess the generality of our findings derived from the THINGS database. Using data from WordNet, our extended analysis demonstrated the strong adaptability of LLMs across concepts differing in concreteness and word classes (Fig. S1a). Consistent results were also observed across various descriptions of the same concept (Fig. S1b). Introducing varying degrees of word order permutations to the query descriptions revealed that LLM predictions were sensitive to linguistic structure degradation when combining words to form concepts (Fig. S1c). These findings highlight the model’s effectiveness in concept inference and its ability to capture at least some of the compositional structure in natural language. Beyond LLaMA3-70B, we tested 66 additional open-source LLMs with different model architectures, scales and training data. The results revealed trends similar to those observed with LLaMA3-70B. They also indicated that larger models generally perform better and more effectively leverage contextual cues for concept inference (Supplementary Information SI 1.1, Fig. S1d-f).

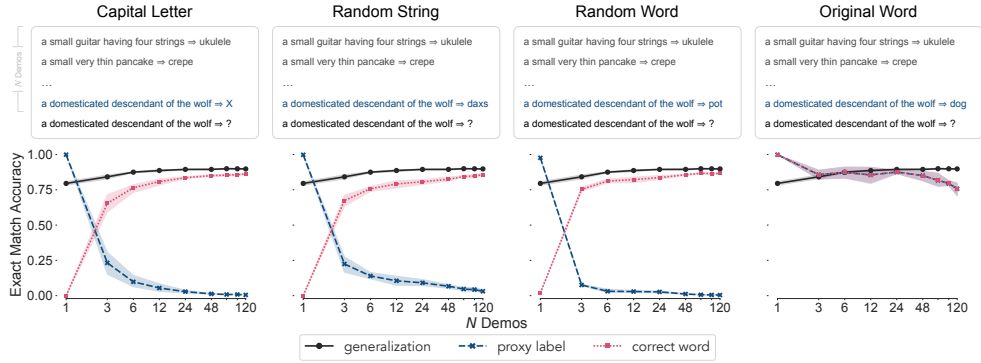


**Fig. 2** Performance of LLaMA3-70B on the reverse dictionary task measured through exact match accuracy. Across the four plots, the black lines denote the model’s performance when presented with  $N$  demonstrations sampled from the training set and evaluated on an independent test set. The blue and red lines illustrate the model’s behavior when presented with one misleading demonstration—a description paired with a proxy label (as specified in the figure titles)—and  $N-1$  correct demonstrations of other concepts. The blue line shows the frequency with which the model copies the misleading demonstration and reproduces the proxy label, while the red line indicates how often it generates the correct word for the query concept given contextual information from other concepts. Shaded areas denote 95% bootstrapped confidence intervals, calculated from 10,000 resamples over five independent runs.

### 2.3 Uncovering a context-independent conceptual structure

To uncover how concepts are represented and organized within LLMs, we looked into the representation spaces they constructed for concept inference and analyzed the interrelationships among the conceptual representations. We characterized the representation spaces formed under different contexts by their relational structure, captured through a (dis)similarity matrix, and measured pairwise alignment by correlating these matrices [43, 44] (Methods 4.3). For concepts in the THINGS database, the alignment between representation spaces gradually increased as the number of demonstrations rose from 1 to 24, with diminishing gains beyond this threshold (Fig. 3a). The alignment with the space formed by 120 demonstrations increased from 0.800 ( $\pm 0.017$ ) with one demonstration to 0.970 ( $\pm 0.003$ ) after 24 demonstrations. This alignment demonstrated a strong correlation with the model’s exact match accuracy on concept inference ( $\rho = 0.976$ ,  $P < 0.0001$ , 95% CI: 0.730–1.0) (Fig. 3b). These results suggest that LLMs are able to construct a coherent and context-independent relational structure, which is reflected in their concept inference capacity. Additional metrics corroborated this conclusion (Methods 4.3 and Supplementary Information SI 1.2), highlighting that intricate relationships among concepts are consistently preserved within LLMs’ representation spaces across varying contexts. This invariance supports the generalization of knowledge encoded in these relationships.

To examine whether different LLMs trained for language prediction can develop similar conceptual representations, we compared the representation spaces they formed based on 24 demonstrations. Using t-SNE [45], we visualized pairwise alignments between models and observed that LLMs with over 70% exact match accuracy on

concept inference clustered closely, whereas those with accuracy below 50% exhibited greater dispersion (Fig. 3c). This indicates that better-performing models share more similar relational structure of concepts, while those with weak performance diverge in their own ways. Further supporting this observation, a correlational analysis demonstrated that models with higher exact match accuracy aligned more closely with representations derived from LLaMA3-70B ( $\rho = 0.870$ ,  $P < 0.0001$ , 95% CI: 0.756–0.940; Fig. 3d). Additionally, when quantifying model complexity based on scale and training data (Methods 4.4), we found that higher-complexity LLMs tended to align better with LLaMA3-70B, though exceptions likely stemmed from constraints in model scale or training data quality (Fig. 3d). These findings suggest that, with sufficient model scale and extensive, high-quality training data, LLMs can converge towards a shared conceptual structure. This convergence, reflected in their concept inference capacity, arises naturally from language prediction without real-world reference.

## 2.4 Predicting various facets of human concept usage

Next, we investigated how well the conceptual representations and structures derived from LLMs align with various aspects of human concept usage. Specifically, we used these representations to predict human behavioral data across three key psychological phenomena: similarity judgments, categorization and gradient scales along various features. To evaluate their effectiveness, we compared the LLM-derived representations against traditional static word embeddings learned from word co-occurrence patterns [46].

For similarity judgments, we compared LLM-derived conceptual representations with human similarity ratings for concept pairs from SimLex-999 [47], which has proven challenging for traditional word embeddings. We also complemented our analysis using human triplet odd-one-out judgments from the THINGS-data collection [40], which relied on image-based rather than text-based stimuli and introduced a contextual effect through the third concept. As shown in Fig. 4a, similarity scores derived from LLM representations strongly correlated with human ratings in SimLex-999, with the correlation improving as the number of contextual demonstrations increased ( $\rho = 0.776 \pm 0.007$  with 72 demonstrations across five runs,  $P < 0.0001$ ). These representations significantly outperformed traditional word embeddings, which achieved a correlation of  $\rho = 0.464$  ( $P < 0.0001$ ). For THINGS triplets, we calculated pairwise similarities to identify the odd-one-out (Methods 4.5). The LLM prediction accuracy also improved with increasing contextual demonstrations, plateauing at 63.20% ( $\pm 0.29\%$ ) after 48 demonstrations (Fig. 4b). This performance closely approached the noise ceiling estimated from individual behavior ( $67.67\% \pm 1.08\%$ ) and substantially exceeded that of word embeddings (48.10%). These findings suggest that, within proper context, the conceptual representations formed by LLMs effectively support the computation of similarities, a core property of human concepts.

We then examined whether categories can be induced from the relative similarity between LLM-derived conceptual representations, using the human-labeled high-level categories from the THINGS database [42]. Applying a prototype-based categorization approach (Methods 4.6), we observed that LLM-derived representations consistently achieved high accuracy, reaching 92.25% ( $\pm 0.15\%$ ) with only 24 demonstrations,

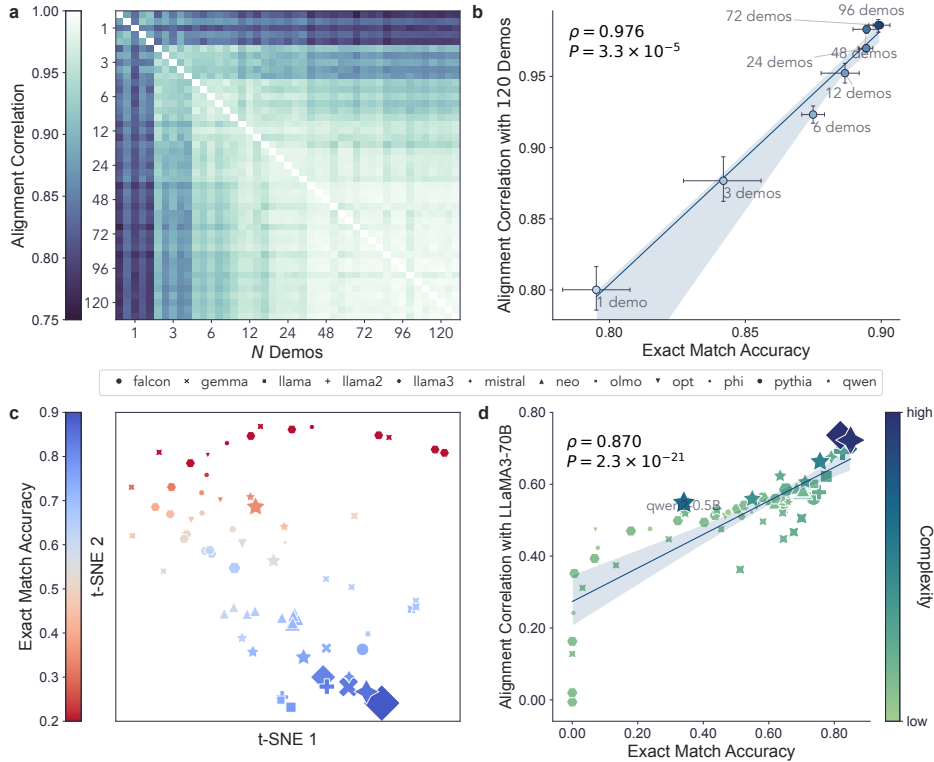


**Fig. 3** LLMs converge toward a similar representational structure of concepts. **a**, Alignment correlation (RSA) between the LLM-derived conceptual representations across different contextual demonstrations. The LLM (LLaMA3-70B) is presented with  $N$  demonstrations, repeated across five independent runs. **b**, LLM performance on the reverse dictionary task reflects alignment with the representations formed based on 120 demonstrations. Each point corresponds to the representations formed by the LLM based on  $N$  demonstrations, with the x-axis indicating exact match accuracy and the y-axis denoting the alignment correlation. Error bars indicate 95% confidence intervals, calculated using 10,000 bootstrap resamples from five independent runs. **c**, A t-SNE visualization of conceptual representations produced by different LLMs. Each point corresponds to an LLM, with representations formed based on 24 demonstrations. Distances between them are calculated as  $1 - \text{alignment}$ , with results averaged over five independent runs. LLMs are plotted in proportion to their complexity and color-coded by their exact match accuracy on the reverse dictionary task. Better-performing models (blue) exhibit more aligned representations. **d**, LLMs’ concept inference capacity reflects alignment correlation with conceptual representations derived from LLaMA3-70B. The x-axis represents the average performance on the reverse dictionary task with 24 demonstrations, while the y-axis indicates the alignment correlation with LLaMA3-70B representations. Data points correspond to conceptual representations derived from different models and are color-coded by model complexity. Linear fits are shown as straight lines, with shaded areas representing 95% confidence intervals derived from 10,000 bootstrap resamples. Overall, models with higher complexity align more closely with the reference. An exception is Qwen2-0.5B, which, despite exhibiting relatively high complexity, has a low alignment score. This may be due to constraints in model scale and the quality of training data.

significantly outperforming static word embeddings (77.88%) (see Supplementary Information SI 1.4 and Fig. S3c). A t-SNE visualization of these representations



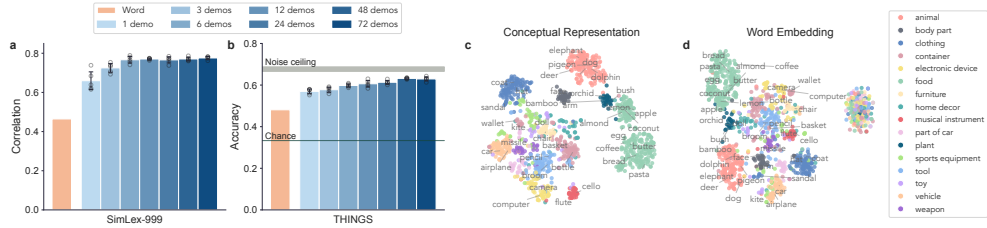


**Fig. 4** Evaluation of alignment between LLM-derived conceptual representations and psychological measures of similarity. **a–b**, Performance of LLaMA3-70B conceptual representations compared to static word embeddings (Word) in predicting human similarity judgments. **a**, Performance on human similarity ratings for concept pairs from SimLex-999, evaluated by Spearman’s rank correlation. **b**, Performance on human triplet odd-one-out similarity judgments in THINGS, measured by prediction accuracy. The noise ceiling reflects the upper bound of performance based on individual response consistency for the same triplet. Error bars and shaded regions represent 95% confidence intervals calculated from five independent runs. **c–d**, t-SNE plots of LLM-derived conceptual representations (**c**) and static word embeddings (**d**). Data points are color-coded based on human-labeled categories from THINGS. Conceptual representations derived from LLaMA3-70B show a clear alignment with category structure, in contrast to the less distinct clustering observed with word embeddings.

revealed notable differences in their similarity structures (Fig. 4c–d). The LLM-derived conceptual representations formed distinct clusters corresponding to high-level categories, such as animals and food, while word embeddings exhibited less distinct category separation. Furthermore, LLM representations revealed broader distinctions, separating natural and animate concepts from man-made and inanimate ones. Among these groupings, human body parts clustered more closely with man-made objects than other animals do, while processed food appeared closer to natural and animate objects. These patterns align with previous findings on human mental representations [48] and are prominent in LLM representations, underscoring the meaningful correspondence between LLM-derived conceptual structures and human knowledge.

Finally, we investigated whether LLM conceptual representations could capture gradient scales of concepts along various features. For example, on a scale of 1 to 5 relative to other animals, CHEETAHS might rank a 5 for speed but fall closer to 3 for size. Using LLM-derived representations for such ratings, we predicted human behavioral data across 52 category-feature pairs (e.g., animals rated for speed) [49] (Methods 4.7). The results (Fig. 5) revealed strong correlations with human ratings ( $\rho > 0.5$ ,  $P < 0.001$ , FDR controlled) for 48 out of 52 category-feature pairs, with a median correlation of 0.817 (95% CI: 0.777–0.851) across all pairs. When accounting for the split-half reliability of human ratings (median  $\rho = 0.954$ ), the median correlation reached 0.871 (95% CI: 0.841–0.891). Among the three category-feature pairs without statistically significant correlations (FDR  $P > 0.01$ ), two exhibited marginal significance (FDR  $P < 0.05$ ), while the weakest correlation appeared in the rating of clothing by age. As shown in Fig. 6, the LLM conceptual representations outperformed static word embeddings [49] across most category-feature pairs. This advantage remained robust after excluding concepts with extreme feature values from the correlation analysis (Supplementary Information SI 1.5), confirming that the success of LLMs is not driven by outlier items. Our findings demonstrate that LLM-derived conceptual

representations advantageously handle intricate human knowledge across diverse object categories and features, highlighting their potential to advance our understanding of conceptual representations in the human mind.

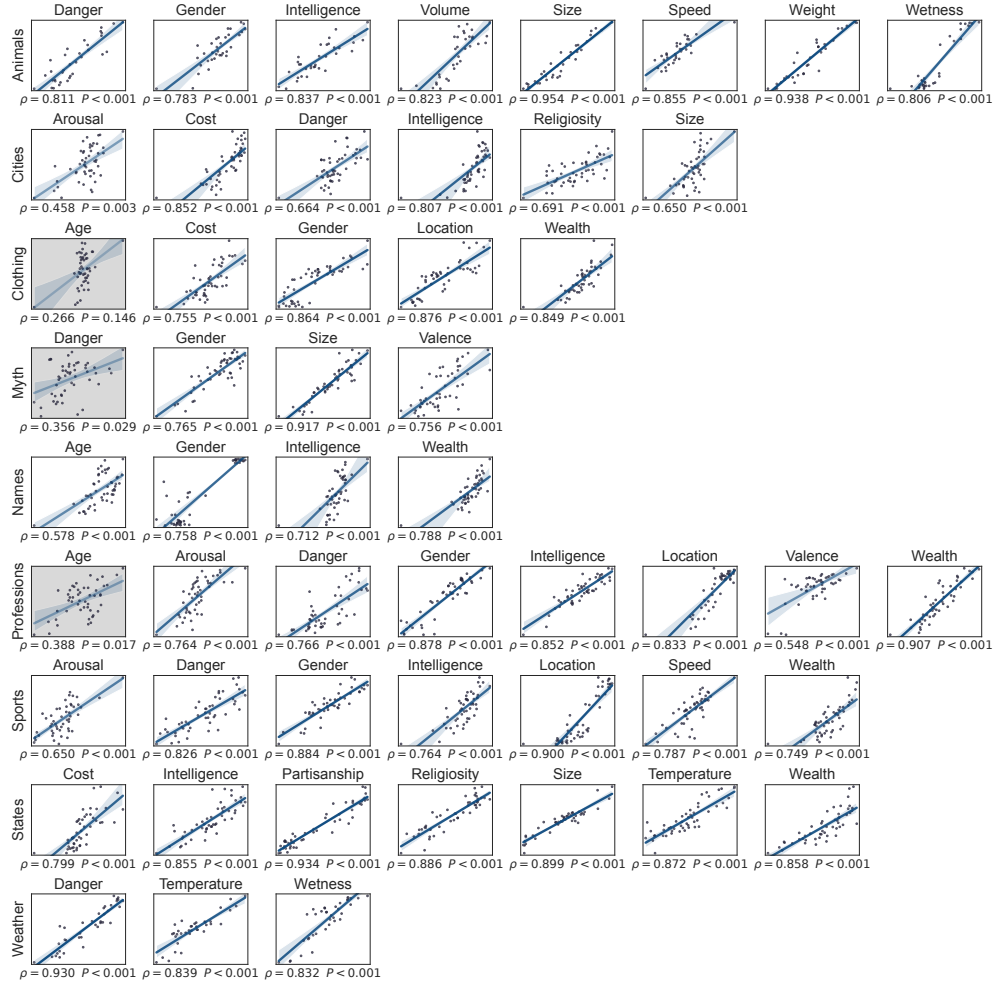


**Fig. 5** Performance of conceptual representations derived from LLaMA3-70B in predicting context-dependent human ratings across 52 category-feature pairs. Scatter plots illustrate the relationship between predicted ratings from conceptual representations (x-axis) and the average human ratings (y-axis). Linear fits are shown as straight lines, with shaded regions representing 95% confidence intervals derived from 10,000 bootstrap resamples. Category-feature pairs with statistically significant correlations (Spearman’s rank correlation,  $P < 0.01$ , FDR controlled) are displayed against a white background.

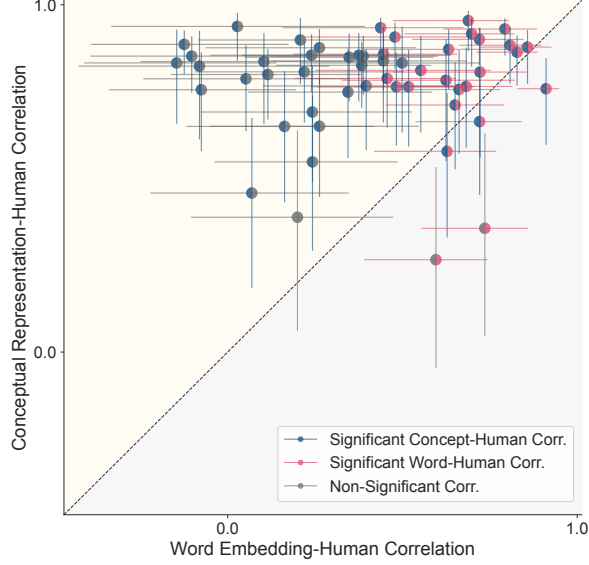


**Fig. 6** Comparison of LLM-derived conceptual representations and static word embeddings in predicting context-dependent human ratings. The x-axis represents correlations with human ratings based on static word embeddings, while the y-axis represents correlations based on conceptual representations derived from LLaMA3-70B. Colored points indicate significant correlations (Spearman’s rank correlation, FDR  $P < 0.01$ ). Error bars represent 95% confidence intervals estimated from 10,000 bootstrap resamples.

## 2.5 Mapping to activity patterns in the human brain

We further explored the biological plausibility of LLM-derived conceptual representations by mapping them onto the activity patterns in the human brain. Using fMRI data from the THINGS-data collection [40], we fitted a voxel-wise linear encoding model to predict neural responses evoked by viewing concept images, based on the corresponding conceptual representations derived from LLaMA3-70B (Methods 4.9). Fig. 7a–c shows the prediction performance maps, indicating voxels where the predicted activations best correlated with actual activations ( $P < 0.01$ , FDR controlled). The LLM-derived conceptual representations successfully predicted activity patterns across widely distributed brain regions, encompassing the visual cortex and beyond. In particular, category-selective regions were more strongly represented, including the lateral occipital complex (LOC), occipital face area (OFA), fusiform face area (FFA), parahippocampal place area (PPA), extrastriate body area (EBA) and medial place area (MPA). These patterns are consistent with prior work suggesting that abstract semantic information was primarily represented in the higher-level visual cortex [50–53]. Meanwhile, significant prediction performance was observed in early visual regions, including V1, indicating that information processed in low-level visual areas is also relevant and can be effectively inferred by LLMs trained exclusively on language data. The consistent location of informative voxels across participants supports the generality of our findings (Fig. S6a–c).

To better understand the alignment between LLM-derived conceptual representations and neural coding of concepts, we compared these representations with two baselines: (1) widely adopted static word embeddings trained via fastText, as in the previous section, and (2) a similarity embedding [40, 48] trained on and validated to successfully account for human similarity judgments for the THINGS concepts. For each baseline, we applied singular value decomposition (SVD) to reduce the dimensionality of the LLM-derived conceptual representations to match that of the baseline. We then combined both representations and used variance partitioning to disentangle their contributions (Methods 4.10), thereby rigorously assessing the efficacy of LLM-derived conceptual representations.

As shown in Fig. 7d–f, LLM-derived conceptual representations and the similarity embedding shared a considerable amount of explained variance, particularly within higher-level visual areas, with some overlap in early visual regions. This indicates that both accounted well for neural responses associated with visual concepts. However, the analysis of unique variance revealed that LLM-derived conceptual representations captured a greater proportion of variance, extending from higher-level regions to early visual areas including V1 (Fig. 7d). By comparison, the unique variance explained by the similarity embedding was primarily concentrated in low-level regions, with limited contributions in higher-level areas such as hV4 and EBA (Fig. 7e). This difference was even more pronounced when leveraging the full dimensionality of LLM-derived conceptual representations for analysis (Supplementary Information SI 1.6). These findings suggest that the brain’s encoding of concepts transcends mere similarities, with some information better captured by the conceptual representations formed by LLMs in context. Nevertheless, certain aspects of visual information relevant to human behavior may not be adequately represented in these representations learned solely from language.

Compared to static word embeddings, LLM-derived conceptual representations alone accounted for a substantially larger portion of explained variance across the visual system (Fig. 7g), while word embeddings contributed minimal uniquely explained variance (Fig. 7h). Moreover, limited shared variance was observed between the two representations, spanning visual areas such as V1, hV4, and FFA (Fig. 7i). These results suggest that LLM-derived conceptual representations capture richer and more nuanced information than static word embeddings, supporting the idea that neural encoding of concepts extends beyond information encapsulated in static word forms. Overall, our findings demonstrate that LLM-derived conceptual representations offer a compelling model for understanding how concepts are represented in the brain.

### 3 Discussion

In this paper, we demonstrated that next-token prediction over language naturally gives rise to human-like conceptual representations and organization, even without real-world grounding. Our work builds upon the long-explored idea of vectors as conceptual representations [7, 16, 39, 43], while previous work has predominantly focused on word embeddings [27, 49]. We viewed concepts as latent representations used for word generation and guided LLMs to infer them from definitional descriptions. Our findings

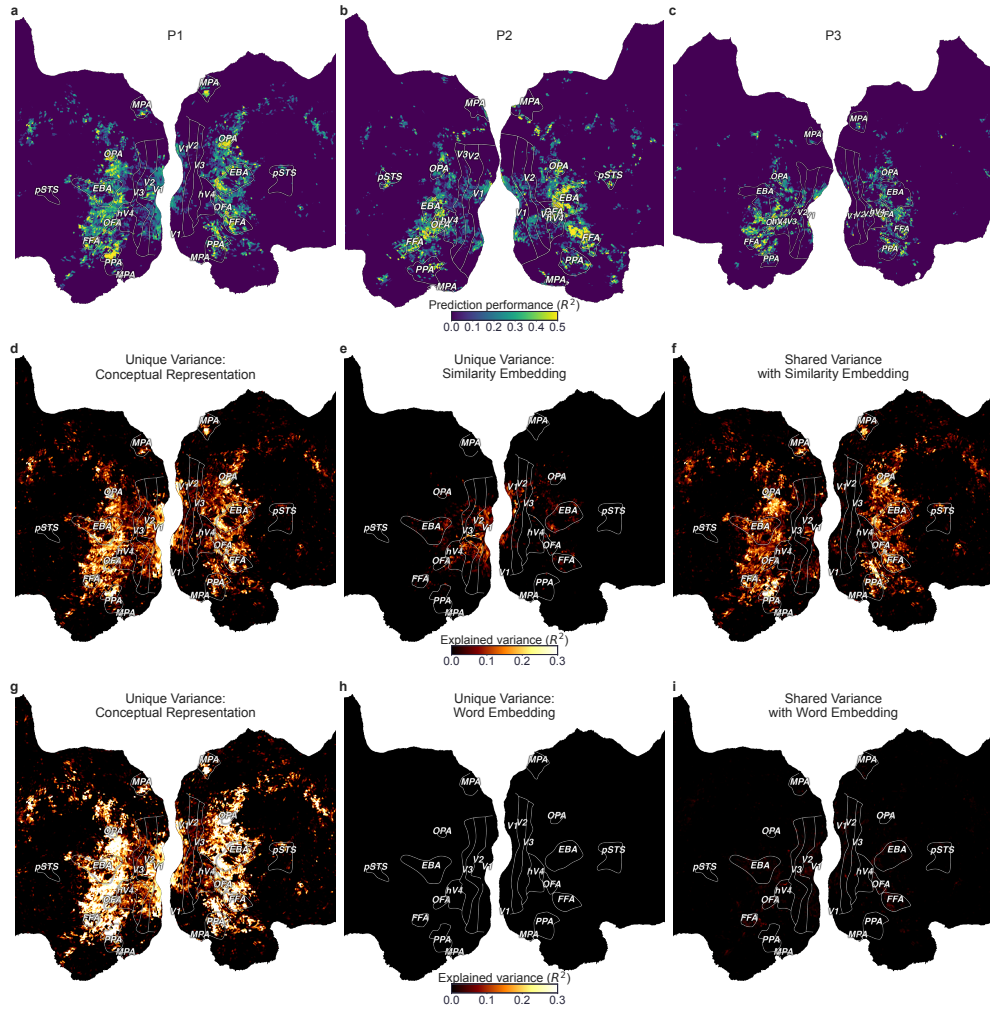


**Fig. 7** Prediction performance of LLM-derived conceptual representation (LLaMA3-70B) and comparison with baseline models in voxel-wise encoding. **a–c**, Prediction performance of LLM-derived conceptual representation visualized on cortical maps for three individual participants. Only voxels with statistically significant correlations between predicted and actual activations are colored (FDR  $P < 0.01$ ). **d–f**, Comparison between LLM-derived conceptual representation and a similarity embedding learned from human similarity judgments. **d**, Variance uniquely explained by the LLM-derived conceptual representation. **e**, Variance uniquely explained by the similarity embedding. **f**, Shared variance explained by both models. **g–i**, Comparison between LLM-derived conceptual representation and a static word embedding (fastText). **g**, Variance uniquely explained by the LLM-derived conceptual representation. **h**, Variance uniquely explained by the static word embedding. **i**, Shared variance explained by both models. The colors represent the proportion of explained variance, normalized relative to the noise ceiling and averaged over five runs.

revealed that LLMs can adaptively derive concepts based on contextual demonstrations, reflecting the interrelationships among them. These representations converged towards a context-independent relational structure predictive of the models’ concept inference capacity, suggesting that language prediction inherently fosters the development of a shared conceptual structure. This structure supports the generalization of knowledge by effectively capturing key properties of human concepts, such as similarity judgments, categorical distinctions and gradient scales along various features. Notably, these conceptual representations showed a strong alignment with neural coding patterns observed in the human brain, even in response to non-linguistic stimuli like visual images. These findings suggest that LLMs serve as promising tools for understanding human conceptual organization. By providing insights into the computational mechanisms underlying conceptual representation, this work establishes a foundation for enhancing the alignment between AI systems and human cognition.

Concepts are considered as mental representations that abstract away specific details and enable flexible generalization in novel situations [3, 4, 17]. Using the reverse dictionary task, we showed that LLMs can effectively derive such conceptual representations from definitional descriptions. While traditional word embeddings have shown potential to capture certain properties required for conceptual representations [36, 49, 54, 55], their capacity is constrained by the inherent context-sensitivity of words, which do not correspond to concepts in a straightforward way [3, 56]. Accordingly, word embeddings are either limited by their static nature—failing to account for context-dependent nuances—or their contextual variability, which precludes consistent mapping to distinct concepts. In contrast, the conceptual representations derived from informative descriptions bypass the ambiguity of words and can be consistently mapped to appropriate terms despite contextual variations (Fig. 2). We argue that these representations are abstract, as their relational structures were consistently preserved across varying contexts (Fig. 3a–b). This consistency indicates that the representations capture the underlying relationships among concepts while discarding surface-level details, a hallmark of abstraction. Such abstraction is essential for generalization, enabling the learned relationships to be flexibly adapted to novel situations. Similar abstract, though disentangled, representations have been observed in humans [57], monkeys [58], rodents [59], and neural networks trained for multitasking [60]. However, the focus on task-specific low-level features is insufficient to model the richness of broadly generalizable real-world concepts. Our results, spanning diverse LLM architectures (Fig. 3c–d), reveal that abstract representations encompassing a wide array of real-world concepts can emerge solely from language prediction. This highlights a promising pathway towards modeling the complexity of the human conceptual repertoire.

Relationships among concepts have long been a cornerstone of cognitive theories [7, 14, 43]. Here, we showed that language prediction naturally gives rise to interrelated concepts. This is demonstrated through the concept inference behavior of LLMs, which was shaped by contextual cues rather than occurring in isolation (Fig. 2), and the consistently preserved relational structure within their representation spaces (Fig. 3a–b). Comparisons with human data further revealed that these relationships aligned with psychological measures of similarity and encapsulated a wealth of human conceptual knowledge (Fig. 4 and Fig. 5). According to conceptual role semantics (CRS) [61, 62],

the meaning of a concept is determined by its relationships to other concepts and its role in thinking, rather than reference to the real world. It has been claimed that LLMs may possess human-like meaning in this sense, with language serving as a valuable source for inferring how people use concepts in thought [38]. However, evidence was needed to determine whether the objective of language prediction can lead to the discovery of the right conceptual roles. Our results support this claim, showing that the relationships among LLM-derived conceptual representations approximate human meaning. While these relationships could be further refined to match those of humans, particularly with respect to real-world grounding, compositionality and abstract reasoning [27, 63], our findings suggest that LLMs offer a prospective computational footing for implementing conceptual role semantics, paving the way for the development of more human-like, concept-based AI systems.

Moreover, we observed that LLMs converged on a shared relational structure of concepts (Fig. 3c–d), aligning with the recently proposed “Platonic Representation Hypothesis” [64]. This hypothesis posits that AI models, despite differing training objectives, data, and architectures, will converge on a universal representation of reality. Our findings provide evidence for this hypothesis by elucidating the representational structure of concepts emerging from language prediction over massive amounts of text. They complement previous observations of nascent alignment among models trained on different modalities [64] and lay the groundwork for concept-based alignment across modalities, between AI systems, and between AI and humans [65].

Theories of concepts have identified various properties that conceptual representations must satisfy, highlighted by the symbolism-connectionism divide. Our results show that LLM-derived conceptual representations successfully reconcile the seemingly competing properties, integrating the definitions, relations and structures emphasized by the symbolic approaches with the graded and continuous nature of neural networks. These representations were structured in a way that their relationships supported straightforward computations of human-like similarities, categories (Fig. 4, Supplementary Information SI 1.4) and gradient distinctions (Fig. 5). Previous work has employed distributed word embeddings to approximate these aspects of human concept usage, revealing preliminary correspondence [47, 49, 54]. However, these embeddings have exhibited inconsistent alignment with human similarity judgments across various datasets [27]. Our results align with previous findings, showing that word embeddings primarily reflect association or relatedness but fail to capture genuine similarity (Fig. 4a–b, Supplementary Information SI 1.3). In contrast, LLM-derived conceptual representations demonstrated distinctive strengths. They excelled in modeling human similarity judgments, including those based on images, suggesting that they advantageously capture conceptual information independent of stimulus modality. These representations also supported flexible, context-dependent reorganization to reflect gradient scales along different features, surpassing word embeddings in both breadth and depth. Importantly, they exhibited superior alignment with neural activity patterns in the human brain (Fig. 7). Collectively, these findings underscore the potential of LLM-derived conceptual representations to advance our understanding of human concepts and to bridge the long-standing divide between symbolic and connectionist approaches.

Vector-based models have been argued to plausibly capture the neural activations underlying actual cognitive processes in the brain [8, 16]. The mapping between LLM-derived conceptual representations and brain activity patterns suggests that they provide a plausible basis for analyzing neural representations of concepts (Fig. 7). Compared to word embeddings and representations derived from human similarity judgments, the LLM-derived representations exhibited notable advantages, especially in accounting for neural activity patterns in high-level visual regions (Fig. 7d-i) that are associated with abstract semantic information [50, 51, 53]. However, they fell short in capturing certain aspects of behaviorally relevant, low-level visual information (Fig. 7d-f). To understand this discrepancy, we regressed the similarity representations onto the LLM-derived representations and found the most pronounced gaps in factors related to color, followed by texture and shape, which are primarily perceptual properties (Supplementary Information SI 1.6, Fig. S11). This result aligns with previous research showing that blind individuals primarily acquire such properties through inference and differ significantly from sighted people in their knowledge of color [37, 66]. Such information, therefore, may be inefficient to learn from language or even absent altogether. Despite these limitations, the substantial alignment between LLM-derived representations and neural responses to visual stimuli adds to the evidence that language prediction can orient models towards a shared representational structure of reality, even in the absence of real-world grounding [36, 64]. While prior work has hinted at this convergence [67], our findings explicitly characterize the conceptual structure emerging solely from language, setting the stage for future research on the alignment and interaction between linguistic and visual systems.

Our work provides a foundational framework for exploring the emergence of conceptual representations from language prediction. We demonstrated that deep neural networks, trained for next-token prediction at sufficient scale and with extensive high-quality training data, can develop abstract conceptual representations that converge toward a shared, context-independent relational structure, enabling generalization. Despite the lack of real-world reference, these representations reconcile essential properties of human concepts and plausibly reflect neural representations in the brain associated with visually grounded concepts. These findings position LLMs as powerful tools for advancing theories of concepts. However, unlike human cognition that relies on concepts for understanding and reasoning, LLMs operate at the token level and do not necessarily utilize the conceptual representations during typical text generation. This discrepancy may lead to the observed limitations of LLMs in certain aspects of concept usage, such as compositionality [27] and reasoning [4, 21].

Future work could aim to build better models of human cognition by incorporating more cognitively plausible incentives [68] such as systematic generalization [69] and reasoning [70–72], while explicitly guiding models to leverage conceptual representations, rather than linguistic forms, to generalize across tasks. Recent progress in steering LLMs to operate within their representation spaces have shown promise in enhancing both language generation and reasoning [73, 74]. Efforts in this direction could narrow the gaps between LLMs and human conceptual abilities and help elucidate their current limitations in compositionality [27], reasoning [4, 21] and over-sensitivity to minor contextual shifts [21, 75]. Moreover, the LLM-derived conceptual representations could



be enriched with information from diverse sources, like vision [63, 76], to better align with human cognition [65] and foster human-machine collaboration [77, 78]. Finally, incorporating brain data beyond the visual domain would offer a richer understanding of the neural underpinnings of conceptual representations in the human mind. Despite the current limitations in models and data, the emergence of human-like conceptual representations within LLMs marks a critical step towards resolving enduring questions in the science of human concepts. This progress opens new avenues for bridging the gaps between human and machine intelligence, offering valuable insights for both cognitive science and artificial intelligence.

## 4 Methods

### 4.1 Large language models used in our experiments

This paper focuses on base models, i.e., LLMs pretrained solely for next-token prediction without fine-tuning or reinforcement learning. Our experiments exclusively utilized open-source LLMs, as their hidden representations are necessary for our analysis. We primarily conducted our experiments on the LLaMA 3 models, including LLaMA3-70B and LLaMA3-8B, both trained on over 15 trillion tokens [79]. Another 11 series of Transformer-based decoder-only LLMs were also employed for experiments on the reverse dictionary task and the convergence of LLM representations. These included (1) Falcon [80], (2) Gemma [81], (3) LLaMA 1 [82], (4) LLaMA 2 [83], (5) Mistral [84, 85], (6) MAP-Neo [86], (7) OLMo [87], (8) OPT [88], (9) Phi [89], (10) Pythia [90], and (11) Qwen [91, 92]. Additional details about the models’ names, scales, training data and sources can be found in Table S1 and Table S2. These models vary in architecture, scale, and pretraining data, enabling explorative analyses of how these factors might impact the conceptual representations and organization within LLMs.

### 4.2 Details on deriving conceptual representations

We used data from the THINGS database [42] to probe LLMs’ conceptual representations via the reverse dictionary task. The dataset includes 1,854 concrete and nameable object concepts, paired with their WordNet synset IDs, definitional descriptions, several linked images and category membership labeled by humans. The concepts and images were selected to be representative of everyday objects commonly used in American English, providing a useful testbed for analyzing model representations. To assess the generality of our results, we extended our analysis to a broader range of descriptions and concepts. Specifically, (1) we tested LLMs’ generalizability across different word classes (nouns, verbs, adjectives and adverbs), age-of-acquisition, and degrees of concreteness using a broader set of 21,402 concepts. The concepts were selected from the intersection of the three datasets: age-of-acquisition [93], concreteness [94] and Wordnet [95]. (2) We evaluated the consistency of LLMs’ predictions using three additional distinct definitional descriptions for each of the 1,854 THINGS concepts, which were generated by GPT-3.5 and manually checked for diversity (see Supplementary Information SI 2.1 for details). (3) We examined LLMs’ sensitivity to linguistic structure by introducing varying degrees of word order permutations to the query

descriptions. We shuffled 30%, 60% and 100% of the words in the query descriptions from the THINGS database and reinserted them into the original text.

To guide LLMs in the reverse dictionary task [96], we selected a random 20% subset of concepts as the training set (from THINGS for most analyses and WordNet data for the 21,402 WordNet concepts), with the remaining concepts comprising the test set. From the training set,  $N$  description-word pairs were randomly chosen as demonstrations. Model performance was evaluated based on strict exact matches across five independent runs, each with a unique random selection of  $N$  demonstrations. For each test concept, we prompted an LLM with a specific description followed by the arrow symbol “ $\Rightarrow$ ” and truncated the output at the first newline character (“ $\backslash n$ ”). We then assessed whether the resulting output matched the expected word or any listed synonyms in THINGS (or WordNet). We opted for greedy search as our decoding method for a straightforward and equitable comparison across models. For subsequent representational analyses, we extracted conceptual representations from the penultimate layer of LLMs at the arrow symbol “ $\Rightarrow$ ”, which directly yielded subsequent predictions, bridging phrasal and lexical terms within the models.

To probe the interrelatedness among concepts within LLMs, we examined how modifying the description-word pairings in context affects model inferences. For each target concept, we paired its description with a proxy symbol and combined it with  $N - 1$  correct description-word pairs from other concepts. We then queried the LLM using the same description. Model performance was evaluated based on how often the LLM replicated the proxy symbol or generated the correct word for the target concept. We tested four types of proxy symbols: (1) a random uppercase English letter, excluding “A” and “I” to avoid potential semantic associations; (2) a randomly generated lowercase letter string, with length sampled from a shifted Poisson distribution (mean = 6.94, variance = 5.80) to approximate typical English word lengths [97]; (3) a random word selected from the THINGS database, distinct from the target concept and absent from the given context; and (4) the correct word for the target concept, used as a baseline.

### 4.3 Structural analysis of representation spaces

We used representational similarity analysis (RSA) [44] to measure the alignment between conceptual representations derived under different conditions (i.e., varying contexts or models), which is non-parametric and has been widely adopted to measure topological alignment between representation spaces [98]. Let  $X \in \mathbb{R}^{m \times d_1}$  and  $Y \in \mathbb{R}^{m \times d_2}$  denote two sets of conceptual representations for  $m$  concepts with dimensionality of  $d_1$  and  $d_2$ , respectively. Each space is characterized by its relational structure, represented by a (dis)similarity matrix  $M \in \mathbb{R}^{m \times m}$ , where the entry  $M_{i,j}$  denotes the (dis)similarity between the representations of the  $i^{\text{th}}$  and  $j^{\text{th}}$  concepts in the corresponding space. The alignment can then be calculated as the Spearman’s rank correlation between the upper (or lower) diagonal portion of the two matrices  $M_X$  and  $M_Y$ , yielding values ranging from  $-1$  to  $1$ .

An appropriate similarity function is needed for the (dis)similarity matrix to characterize the relational structure of the representation space. While cosine similarity has been widely adopted since the advent of static distributed word embeddings, it may be suboptimal for capturing non-linear relationships and sensitive to outliers [99]. We

thus employed two different metrics including the cosine similarity and Spearman’s rank correlation. Comparison with human behavioral data suggests that the cosine similarity captures semantic similarity (e.g., CUPS and MUGS) while Spearman’s rank correlation reflects both similarity and association (e.g., CUPS and COFFEE) (Supplementary Information SI 1.3, Fig. S3a–b). We primarily used Spearman’s rank correlation as the similarity function, with results from alternative metrics provided in Supplementary Information SI 1.2.

Additionally, we employed the parallelism score (PS) [58] to evaluate if the differences between conceptual representations are preserved across conditions, which have been thought to reflect relations in the representation space [49, 100]. The PS for each concept pair, among the total  $m$  concepts, is computed as the cosine similarity between the vector offsets from one concept to the other. We reported the average PS for two representation spaces (Supplementary Information SI 1.2, Fig. S2c–d).

For comparison across different LLMs, we also visualized these models using t-SNE with a perplexity of 30 and 1000 iterations, where distances were computed as 1 – alignment.

#### 4.4 Characterization of model complexity

For a general characterization of the complexity of the 67 LLMs used in our experiments, we represented each by its number of parameters and amount of training data (i.e., the number of tokens used during training)—factors identified as crucial for determining model quality [101, 102]. A principal component analysis (PCA) was then applied to these factors. The first principal component, accounting for 70.67% of the total variance, was used to represent the complexity of each model. In terms of the Mistral models, where information about their pretraining data was not accessible, we estimated it based on the data volume of comparable models released around the same time (Table S1).

#### 4.5 Prediction of human similarity judgments

To evaluate how closely the relationships between LLM-derived representations align with psychological measures of similarity, we first compared them with human similarity ratings for concept pairs from SimLex-999 [47]. The dataset explicitly distinguishes semantic similarity from association or relatedness and contains human ratings for 999 concept pairs spanning 1,028 concepts. The concepts cover three word classes including nouns, verbs and adjectives. We used description-word pairs from the WordNet data to provide contextual demonstrations to the LLMs, thereby deriving conceptual representations. Model performance was assessed through Spearman’s rank correlation between the similarity scores derived from the LLM representations and the human ratings.

We further employed the odd-one-out similarity judgments from the THINGS-data collection [40] to validate the effectiveness of LLM representations in handling the computation of similarities. The dataset consists of triplets sampled from the 1,854 concepts in THINGS. We presented LLMs with contextual demonstrations randomly sampled from THINGS to obtain their conceptual representations. For each triplet  $(i, j, k)$ , we took the corresponding conceptual representations  $(\mathbf{h}_i, \mathbf{h}_j, \mathbf{h}_k)$  and

calculated pairwise similarity. The one outside the most similar pair was identified as the odd-one-out and compared to human judgments. We evaluated model performance mainly with a set of 1,000 triplets from THINGS, each with multiple responses collected from different participants. We compared the LLMs’ judgments with the majority of human choices, which provides a reliable estimation of the alignment between LLMs and humans.

## 4.6 Categorization

For the categorization experiment, we employed high-level human-labeled natural categories in THINGS [42]. We removed subcategories of other categories, concepts belonging to multiple categories and categories with fewer than ten concepts [48]. This resulted in 18 out of 27 categories, including animal, body part, clothing, container, electronic device, food, furniture, home decor, medical equipment, musical instrument, office supply, part of car, plant, sports equipment, tool, toy, vehicle and weapon. These categories comprise 1,112 concepts.

We employed three methods to evaluate the extent to which category membership can be inferred from LLM-derived conceptual representations, with the former two corresponding to prototype and exemplar models and the third explicitly examining the relationships between high-level categories and their associated concepts. Specifically, for the prototype model, we used a cross-validated nearest-centroid classifier, performing categorization by iteratively leaving each concept out. In each iteration, we calculated the centroid for each category by averaging the representations of the remaining concepts. Categorization was then based on the similarity between the left-out concept and each category centroid. In the exemplar model, categorization was carried out using a nearest-neighbour decision rule [103], where each concept was classified based on the category membership of its closest neighbours among all other concepts (Supplementary Information SI 2.2). Our final approach involved constructing a representation for each of the 18 categories using the same  $N$  demonstrations employed for the 1,854 concepts. Here, we directly used the category names as query descriptions, categorizing concepts by their similarity to each category representation.

We combined t-SNE with multidimensional scaling (MDS) to visualize the representations in two dimensions, thereby preserving the global structure while better capturing local similarities. The representations were first reduced to 64 dimensions using MDS, with distances calculated as  $1 - \text{similarity}$  and then visualized using t-SNE with a perplexity of 30 and 1000 iterations.

## 4.7 Prediction of gradient scales along features

To probe whether LLM conceptual representations could also recover detailed knowledge about gradient scales of concepts along various features, we used human ratings spanning various categories and features. The dataset [49] includes 52 category-feature pairs, where participants were asked to rate a concept (e.g., WHALE) within a certain category (e.g., animal) along multiple feature dimensions (e.g., size and danger). The ratings cover nine categories including animals, cities, clothing, mythological creatures, first names, professions, sports, weather phenomena and states of the United States,

with each matched with a subset of 17 features including age, arousal, cost, danger, gender, intelligence, location (indoors versus outdoors), partisanship, religiosity, size, speed, temperature, valence, (auditory) volume, wealth, weight and wetness.

For each category-feature pair, we provided the model with two demonstrations illustrating the extreme values of a target feature within a category. We then queried the model for the rating of each concept in the category to obtain the corresponding representations. For example:

the precise size rating of whales from 1 (small, little, tiny) to 5 (large, big, huge)  $\Rightarrow$  5  
 the precise size rating of ants from 1 (small, little, tiny) to 5 (large, big, huge)  $\Rightarrow$  1  
 the precise size rating of tigers from 1 (small, little, tiny) to 5 (large, big, huge)  $\Rightarrow$  ?

Similar to previous work [49], we constructed a scale vector by subtracting the representation of the minimum extreme from the maximum (e.g.,  $\vec{\text{size}}_{\text{animal}} = \vec{\text{whale}} - \vec{\text{ant}}$ ), and compared all representations to this scale to obtain their relative feature ratings. The performance of LLM-derived representations was then evaluated through the Spearman’s rank correlation between the ratings derived from them and human ratings. For each category-feature pair, we estimated a 95% confidence interval based on 10,000 bootstrap samples. To control for multiple comparisons across the 52 pairs,  $P$ -values were corrected using the false discovery rate (FDR) method.

## 4.8 Word embeddings for comparison

To validate the effectiveness of LLM-derived conceptual representations in capturing human knowledge and to explore their distinct advantages over traditional static word embeddings, we compared them with a state-of-the-art 300-dimensional static word embedding trained through fastText on Common Crawl and Wikipedia [46]. Unlike LLM representations, we used cosine similarity as the similarity measure for the word embeddings, as it consistently aligned better with human behavioral data (Supplementary Information SI 1.3).

The word embeddings were compared with human behavioral data using the same method applied to LLM conceptual representations across all experiments, except for the analysis of gradient distinctions along various features. As static word embeddings do not support context-dependent computations, we followed the procedure in previous work [49] to compute a scale vector based on several antonym pairs denoting opposite values of the target feature. For instance, the opposite values for the feature “size” were represented by  $(\vec{\text{large}}, \vec{\text{big}}, \vec{\text{huge}})$  and  $(\vec{\text{small}}, \vec{\text{little}}, \vec{\text{tiny}})$ , with the scale vector  $\vec{\text{size}}$  calculated as the average of the  $3 \times 3 = 9$  pairwise vector differences between the antonyms. The word embedding for each item was then projected onto this scale vector, and the resulting projections were correlated with human ratings for evaluation.

## 4.9 Encoding model of neural representations in the brain

We used the fMRI dataset from the THINGS-data collection [40] to explore whether LLM conceptual representations can map onto brain activity patterns associated with visually grounded concepts. The dataset encompasses brain imaging data from three participants exposed to 8,740 representative images of 720 concepts over 12 sessions. The concepts are sampled from the total of 1,854 concepts in THINGS and are thus relevant to the behavioral data that can be predicted by LLM conceptual representations. We obtained the neural representation of each concept for each participant by averaging over its corresponding images.

To investigate the relationship between LLM-derived conceptual representations and neural representations, we trained a linear encoding model to predict voxel activations based on the LLM-derived representations. Specifically, the activation at each voxel was modeled by  $y_{v,c} = \mathbf{h}_c \mathbf{w} + b + \epsilon$ , where  $y_{v,c}$  is the activation at voxel  $v$  for concept  $c$ ,  $\mathbf{h}_c$  is the corresponding LLM representation,  $\mathbf{w}$  is a vector of regression coefficients,  $b$  is a constant, and  $\epsilon$  represents residual error. The parameters  $\mathbf{w}$  and  $b$  were estimated via regularized linear regression, minimizing the least-squares error with a ridge penalty controlled by hyperparameter  $\lambda$ , selected through cross-validation within the training set. Model performance was assessed through twenty-fold cross-validation with non-overlapping concepts, evaluating the correlation between predicted and observed neural responses across folds. To establish statistical significance, we generated a null distribution of randomized correlation values from 10,000 test data permutations [104]. Voxel-wise  $P$ -values were computed by comparing predicted correlations to the null distribution and adjusted for multiple comparisons with FDR correction. We also computed noise-ceiling-normalized  $R^2$  for each voxel by dividing the original  $R^2$  by the estimated noise ceiling. The noise ceilings were derived based on signal and noise variance, estimated from neural activity variability to presentations of the same concept [105] (Fig. S12).

## 4.10 Variance partitioning between conceptual and alternative representations

To validate the effectiveness of LLM conceptual representations in explaining neural responses, we compared them against two alternative representations: (1) fastText embeddings as in Methods 4.8 and (2) 66-dimensional similarity embeddings [40] trained on 4.10 million human odd-one-out judgments of concepts in THINGS, which align well with human similarity judgments. These allowed us to examine the additional information encoded in LLM conceptual representations that aligns with human brain activity, beyond word information and similarity.

We combined each baseline representation with LLM-derived conceptual representations and analyzed the shared and unique variance each could account for [104]. To isolate unique variance, we orthogonalized the target representation and the neural responses with respect to the alternate representation, thereby removing the shared variance from both the representation and the fMRI data. The residuals of the target representation were then used to predict the fMRI residuals, and the unique variance explained by the target representation was calculated as the  $R^2$  using twenty-fold

cross-validation. For shared variance, we first concatenated both representations, used them to predict neural responses, and calculated the  $R^2$  in the same twenty-fold cross-validation to determine the total variance explained. Shared variance was subsequently estimated by subtracting the unique contributions of each representation from this total. For our results, we focused on voxels with a noise ceiling greater than 5% and reported the noise-ceiling-normalized  $R^2$ .

**Supplementary information.** The supplementary information contains supplementary text, Figures S1 to S12, and Tables S1 to S2.

**Data and Code Availability.** This work makes use of previously published datasets [40, 42, 46, 47, 49, 95]. The code and additional data for reproducing all our experiments will be made publicly accessible upon publication on GitHub and Zenodo.

## References

- [1] Johnson-Laird, P. N. *Mental models: towards a cognitive science of language, inference, and consciousness* (Harvard University Press, USA, 1986).
- [2] Lake, B. M., Ullman, T. D., Tenenbaum, J. B. & Gershman, S. J. Building machines that learn and think like people. *Behavioral and Brain Sciences* **40**, e253 (2017).
- [3] Murphy, G. *The big book of concepts* (MIT press, 2004).
- [4] Mitchell, M. Abstraction and analogy-making in artificial intelligence. *Annals of the New York Academy of Sciences* **1505**, 79–101 (2021). URL <https://nyaspubs.onlinelibrary.wiley.com/doi/abs/10.1111/nyas.14619>.
- [5] Apostle, H. *Aristotle's Categories and Propositions (De Interpretatione)* (Apostle Translations of Aristotle's Works (Peripatetic Press, 1980).
- [6] Ross, W. *Plato's Theory of Ideas* (Clarendon Press, 1966).
- [7] Shepard, R. N. Toward a universal law of generalization for psychological science. *Science* **237**, 1317–1323 (1987). URL <https://www.science.org/doi/abs/10.1126/science.3629243>.
- [8] McClelland, J. L. *et al.* Letting structure emerge: connectionist and dynamical systems approaches to cognition. *Trends in Cognitive Sciences* **14**, 348–356 (2010). URL <https://www.sciencedirect.com/science/article/pii/S1364661310001245>.
- [9] Tenenbaum, J. B., Kemp, C., Griffiths, T. L. & Goodman, N. D. How to grow a mind: Statistics, structure, and abstraction. *Science* **331**, 1279–1285 (2011). URL <https://www.science.org/doi/abs/10.1126/science.1192788>.

- [10] Mitchell, T. M. *et al.* Predicting Human Brain Activity Associated with the Meanings of Nouns. *Science* **320**, 1191–1195 (2008). URL <https://www.science.org/doi/abs/10.1126/science.1152876>.
- [11] Huth, A. G., de Heer, W. A., Griffiths, T. L., Theunissen, F. E. & Gallant, J. L. Natural speech reveals the semantic maps that tile human cerebral cortex. *Nature* **532**, 453–458 (2016). URL <https://doi.org/10.1038/nature17637>.
- [12] Jackendoff, R. *Foundations of Language: Brain, Meaning, Grammar, Evolution* (Oxford University Press, 2002). URL <https://doi.org/10.1093/acprof:oso/9780198270126.001.0001>.
- [13] Fodor, J. A. *The Language of Thought* (Harvard University Press, 1975).
- [14] Fodor, J. A. & Pylyshyn, Z. W. Connectionism and cognitive architecture: A critical analysis. *Cognition* **28**, 3–71 (1988). URL <https://www.sciencedirect.com/science/article/pii/0010027788900315>.
- [15] Rumelhart, D. E., McClelland, J. L. & Group, P. R. *Parallel Distributed Processing, Volume 1: Explorations in the Microstructure of Cognition: Foundations* (The MIT Press, 1986). URL <https://doi.org/10.7551/mitpress/5236.001.0001>.
- [16] McClelland, J. L. & Rogers, T. T. The parallel distributed processing approach to semantic cognition. *Nature Reviews Neuroscience* **4**, 310–322 (2003). URL <https://doi.org/10.1038/nrn1076>.
- [17] Margolis, E. & Laurence, S. *The Conceptual Mind: New Directions in the Study of Concepts* (The MIT Press, 2015). URL <https://doi.org/10.7551/mitpress/9383.001.0001>.
- [18] Smolensky, P., McCoy, R. T., Fernandez, R., Goldrick, M. & Gao, J. Neurocompositional computing: From the central paradox of cognition to a new generation of ai systems. *AI Magazine* **43**, 308–322 (2022). URL <https://onlinelibrary.wiley.com/doi/abs/10.1002/aaai.12065>.
- [19] Brown, T. *et al.* Larochelle, H., Ranzato, M., Hadsell, R., Balcan, M. & Lin, H. (eds) *Language models are few-shot learners*. (eds Larochelle, H., Ranzato, M., Hadsell, R., Balcan, M. & Lin, H.) *Advances in Neural Information Processing Systems*, Vol. 33, 1877–1901 (Curran Associates, Inc., 2020).
- [20] Jones, C. R. & Bergen, B. K. Does gpt-4 pass the turing test? (2024). Preprint at <https://arxiv.org/abs/2310.20216>.
- [21] Binz, M. & Schulz, E. Using cognitive psychology to understand gpt-3. *Proceedings of the National Academy of Sciences* **120**, e2218523120 (2023). URL <https://www.pnas.org/doi/abs/10.1073/pnas.2218523120>.



- [22] Webb, T., Holyoak, K. J. & Lu, H. Emergent analogical reasoning in large language models. *Nature Human Behaviour* **7**, 1526–1541 (2023). URL <https://doi.org/10.1038/s41562-023-01659-w>.
- [23] Hagendorff, T., Fabi, S. & Kosinski, M. Human-like intuitive behavior and reasoning biases emerged in large language models but disappeared in ChatGPT. *Nature Computational Science* **3**, 833–838 (2023). URL <https://doi.org/10.1038/s43588-023-00527-x>.
- [24] Lampinen, A. K. *et al.* Language models, like humans, show content effects on reasoning tasks. *PNAS Nexus* **3**, pgae233 (2024). URL <https://doi.org/10.1093/pnasnexus/pgae233>.
- [25] Frank, M. C. Openly accessible LLMs can help us to understand human cognition. *Nature Human Behaviour* **7**, 1825–1827 (2023). URL <https://doi.org/10.1038/s41562-023-01732-4>.
- [26] Mitchell, M. & Krakauer, D. C. The debate over understanding in AI’s large language models. *Proceedings of the National Academy of Sciences* **120**, e2215907120 (2023). URL <https://www.pnas.org/doi/abs/10.1073/pnas.2215907120>.
- [27] Lake, B. M. & Murphy, G. L. Word meaning in minds and machines. *Psychological Review* **130**, 401–431 (2023).
- [28] Shiffrin, R. & Mitchell, M. Probing the psychology of ai models. *Proceedings of the National Academy of Sciences* **120**, e2300963120 (2023). URL <https://www.pnas.org/doi/abs/10.1073/pnas.2300963120>.
- [29] Mahowald, K. *et al.* Dissociating language and thought in large language models. *Trends in Cognitive Sciences* **28**, 517–540 (2024). URL <https://www.sciencedirect.com/science/article/pii/S1364661324000275>.
- [30] Ananthaswamy, A. How close is AI to human-level intelligence? *Nature* **636**, 22–25 (2024). URL <https://www.nature.com/articles/d41586-024-03905-1>.
- [31] Bender, E. M. & Koller, A. Jurafsky, D., Chai, J., Schluter, N. & Tetreault, J. (eds) *Climbing towards NLU: On meaning, form, and understanding in the age of data.* (eds Jurafsky, D., Chai, J., Schluter, N. & Tetreault, J.) *Proceedings of the 58th Annual Meeting of the Association for Computational Linguistics*, 5185–5198 (Association for Computational Linguistics, Online, 2020). URL <https://aclanthology.org/2020.acl-main.463>.
- [32] Bender, E. M., Gebru, T., McMillan-Major, A. & Shmitchell, S. Irani, L., Kannan, S., Mitchell, M. & Robinson, D. (eds) *On the dangers of stochastic parrots: Can language models be too big?* (eds Irani, L., Kannan, S., Mitchell, M. & Robinson, D.) *Proceedings of the 2021 ACM Conference on Fairness, Accountability, and Transparency*, FAccT ’21, 610–623 (Association for Computing Machinery, New

- York, NY, USA, 2021). URL <https://doi.org/10.1145/3442188.3445922>.
- [33] Lewis, M. & Mitchell, M. Using counterfactual tasks to evaluate the generality of analogical reasoning in large language models. *Proceedings of the Annual Meeting of the Cognitive Science Society* **46** (2024). URL <https://escholarship.org/uc/item/58d9s666>.
- [34] Dentella, V., Günther, F., Murphy, E., Marcus, G. & Leivada, E. Testing AI on language comprehension tasks reveals insensitivity to underlying meaning. *Scientific Reports* **14**, 28083 (2024). URL <https://doi.org/10.1038/s41598-024-79531-8>.
- [35] Firestone, C. Performance vs. competence in human–machine comparisons. *Proceedings of the National Academy of Sciences* **117**, 26562–26571 (2020). URL <https://www.pnas.org/doi/abs/10.1073/pnas.1905334117>.
- [36] Pavlick, E. Symbols and grounding in large language models. *Philosophical Transactions of the Royal Society A: Mathematical, Physical and Engineering Sciences* **381**, 20220041 (2023). URL <https://royalsocietypublishing.org/doi/abs/10.1098/rsta.2022.0041>.
- [37] Kim, J. S., Aheimer, B., Manrara, V. M. & Bedny, M. Shared understanding of color among sighted and blind adults. *Proceedings of the National Academy of Sciences* **118**, e2020192118 (2021). URL <https://www.pnas.org/doi/abs/10.1073/pnas.2020192118>.
- [38] Piantadosi, S. & Hill, F. Meaning without reference in large language models (2022). URL <https://openreview.net/forum?id=nRkJEwmZnM>. Paper presented at NeurIPS 2022 Workshop on Neuro Causal and Symbolic AI (nCSI).
- [39] Piantadosi, S. T. *et al.* Why concepts are (probably) vectors. *Trends in Cognitive Sciences* **28**, 844–856 (2024). URL <https://doi.org/10.1016/j.tics.2024.06.011>. Publisher: Elsevier.
- [40] Hebart, M. N. *et al.* Things-data, a multimodal collection of large-scale datasets for investigating object representations in human brain and behavior. *eLife* **12**, e82580 (2023). URL <https://doi.org/10.7554/eLife.82580>.
- [41] Zock, M. & Bilac, S. Word lookup on the basis of associations : from an idea to a roadmap (2004). URL <https://aclanthology.org/W04-2105>. In Proceedings of the Workshop on Enhancing and Using Electronic Dictionaries, pages 29–35, Geneva, Switzerland, COLING, 2004.
- [42] Hebart, M. N. *et al.* Things: A database of 1,854 object concepts and more than 26,000 naturalistic object images. *PLOS ONE* **14**, 1–24 (2019). URL <https://doi.org/10.1371/journal.pone.0223792>.

- [43] Shepard, R. N. & Chipman, S. Second-order isomorphism of internal representations: Shapes of states. *Cognitive Psychology* **1**, 1–17 (1970). URL <https://www.sciencedirect.com/science/article/pii/0010028570900022>.
- [44] Kriegeskorte, N., Mur, M. & Bandettini, P. A. Representational similarity analysis - connecting the branches of systems neuroscience. *Frontiers in Systems Neuroscience* **2** (2008). URL <https://www.frontiersin.org/journals/systems-neuroscience/articles/10.3389/neuro.06.004.2008>.
- [45] van der Maaten, L. & Hinton, G. Visualizing data using t-sne. *Journal of Machine Learning Research* **9**, 2579–2605 (2008). URL <http://jmlr.org/papers/v9/vandermaaten08a.html>.
- [46] Grave, E., Bojanowski, P., Gupta, P., Joulin, A. & Mikolov, T. Calzolari, N. *et al.* (eds) *Learning word vectors for 157 languages*. (eds Calzolari, N. *et al.*) *Proceedings of the Eleventh International Conference on Language Resources and Evaluation (LREC 2018)* (European Language Resources Association (ELRA), Miyazaki, Japan, 2018). URL <https://aclanthology.org/L18-1550>.
- [47] Hill, F., Reichart, R. & Korhonen, A. SimLex-999: Evaluating semantic models with (genuine) similarity estimation. *Computational Linguistics* **41**, 665–695 (2015). URL <https://aclanthology.org/J15-4004>.
- [48] Hebart, M. N., Zheng, C. Y., Pereira, F. & Baker, C. I. Revealing the multidimensional mental representations of natural objects underlying human similarity judgements. *Nature Human Behaviour* **4**, 1173–1185 (2020). URL <https://doi.org/10.1038/s41562-020-00951-3>.
- [49] Grand, G., Blank, I. A., Pereira, F. & Fedorenko, E. Semantic projection recovers rich human knowledge of multiple object features from word embeddings. *Nature Human Behaviour* **6**, 975–987 (2022). URL <https://doi.org/10.1038/s41562-022-01316-8>.
- [50] DiCarlo, J. J. & Cox, D. D. Untangling invariant object recognition. *Trends in Cognitive Sciences* **11**, 333–341 (2007). URL <https://www.sciencedirect.com/science/article/pii/S1364661307001593>.
- [51] Charest, I., Kievit, R. A., Schmitz, T. W., Deca, D. & Kriegeskorte, N. Unique semantic space in the brain of each beholder predicts perceived similarity. *Proceedings of the National Academy of Sciences* **111**, 14565–14570 (2014). URL <https://www.pnas.org/doi/abs/10.1073/pnas.1402594111>.
- [52] Yamins, D. L. K. *et al.* Performance-optimized hierarchical models predict neural responses in higher visual cortex. *Proceedings of the National Academy of Sciences* **111**, 8619–8624 (2014). URL <https://www.pnas.org/doi/abs/10.1073/pnas.1403112111>.

- [53] Schindler, A. & Bartels, A. Visual high-level regions respond to high-level stimulus content in the absence of low-level confounds. *NeuroImage* **132**, 520–525 (2016). URL <https://www.sciencedirect.com/science/article/pii/S105381191600207X>.
- [54] Hill, F., Cho, K., Korhonen, A. & Bengio, Y. Learning to understand phrases by embedding the dictionary. *Transactions of the Association for Computational Linguistics* **4**, 17–30 (2016). URL <https://aclanthology.org/Q16-1002>.
- [55] Gurnee, W. & Tegmark, M. Language models represent space and time (2024). URL <https://openreview.net/forum?id=jE8xbmvFin>. In 12th International Conference on Learning Representations, Messe Wien Exhibition and Congress Center, Vienna, Austria, 2024.
- [56] Malt, B. C. *et al.* in *Where are the concepts? what words can and can't reveal* (ed. Eric Margolis, S. L.) *The Conceptual Mind: New Directions in the Study of Concepts* 291–326 (The MIT Press, 2015). URL <https://doi.org/10.7551/mitpress/9383.003.0019>. [https://direct.mit.edu/book/chapter-pdf/2271033/9780262326865\\_cak.pdf](https://direct.mit.edu/book/chapter-pdf/2271033/9780262326865_cak.pdf).
- [57] Courellis, H. S. *et al.* Abstract representations emerge in human hippocampal neurons during inference. *Nature* **632**, 841–849 (2024). URL <https://doi.org/10.1038/s41586-024-07799-x>.
- [58] Bernardi, S. *et al.* The geometry of abstraction in the hippocampus and prefrontal cortex. *Cell* **183**, 954–967.e21 (2020). URL <https://www.sciencedirect.com/science/article/pii/S0092867420312289>.
- [59] Boyle, L. M., Posani, L., Irfan, S., Siegelbaum, S. A. & Fusi, S. Tuned geometries of hippocampal representations meet the computational demands of social memory. *Neuron* **112**, 1358–1371.e9 (2024). URL <https://doi.org/10.1016/j.neuron.2024.01.021>.
- [60] Johnston, W. J. & Fusi, S. Abstract representations emerge naturally in neural networks trained to perform multiple tasks. *Nature Communications* **14**, 1040 (2023). URL <https://doi.org/10.1038/s41467-023-36583-0>.
- [61] Greenberg, M. & Harman, G. in *Conceptual role semantics* (eds Lepore, E. & Smith, B. C.) *The Oxford Handbook of Philosophy of Language* 295 (Oxford University Press, 2005).
- [62] Block, N. in *Conceptual role semantics* (ed. Craig, E.) *Routledge Encyclopedia of Philosophy: Genealogy to Iqbal* 242–256 (Routledge, 1996).
- [63] McClelland, J. L., Hill, F., Rudolph, M., Baldridge, J. & Schütze, H. Placing language in an integrated understanding system: Next steps toward human-level performance in neural language models. *Proceedings of the National Academy of Sciences* **117**, 25966–25974 (2020). URL <https://www.pnas.org/doi/abs/10>.

1073/pnas.1910416117.

- [64] Huh, M., Cheung, B., Wang, T. & Isola, P. Salakhutdinov, R. *et al.* (eds) *Position: The Platonic Representation Hypothesis*. (eds Salakhutdinov, R. *et al.*) *Proceedings of the 41st International Conference on Machine Learning*, Vol. 235 of *Proceedings of Machine Learning Research*, 20617–20642 (PMLR, 2024). URL <https://proceedings.mlr.press/v235/huh24a.html>.
- [65] Rane, S., Bruna, P. J., Sucholutsky, I., Kello, C. & Griffiths, T. L. Concept alignment (2024). Preprint at <https://arxiv.org/abs/2401.08672>.
- [66] Kim, J. S., Elli, G. V. & Bedny, M. Knowledge of animal appearance among sighted and blind adults. *Proceedings of the National Academy of Sciences* **116**, 11213–11222 (2019). URL <https://www.pnas.org/doi/abs/10.1073/pnas.1900952116>.
- [67] Wang, A. Y., Kay, K., Naselaris, T., Tarr, M. J. & Wehbe, L. Better models of human high-level visual cortex emerge from natural language supervision with a large and diverse dataset. *Nature Machine Intelligence* **5**, 1415–1426 (2023). URL <https://doi.org/10.1038/s42256-023-00753-y>.
- [68] Irie, K. & Lake, B. M. Neural networks that overcome classic challenges through practice (2024). Preprint at <https://arxiv.org/abs/2410.10596>.
- [69] Lake, B. M. & Baroni, M. Human-like systematic generalization through a meta-learning neural network. *Nature* **623**, 115–121 (2023). URL <https://doi.org/10.1038/s41586-023-06668-3>.
- [70] Zelikman, E., Wu, Y., Mu, J. & Goodman, N. Oh, A. H., Agarwal, A., Belgrave, D. & Cho, K. (eds) *STar: Bootstrapping reasoning with reasoning*. (eds Oh, A. H., Agarwal, A., Belgrave, D. & Cho, K.) *Advances in Neural Information Processing Systems* (2022). URL [https://openreview.net/forum?id=\\_\\_3ELRdg2sgI](https://openreview.net/forum?id=__3ELRdg2sgI).
- [71] OpenAI *et al.* OpenAI o1 system card (2024). Preprint at <https://arxiv.org/abs/2412.16720>.
- [72] Akyürek, E. *et al.* The surprising effectiveness of test-time training for abstract reasoning (2024). Preprint at <https://arxiv.org/abs/2411.07279>.
- [73] team, T. L. *et al.* Large concept models: Language modeling in a sentence representation space (2024). Preprint at <https://arxiv.org/abs/2412.08821>.
- [74] Hao, S. *et al.* Training large language models to reason in a continuous latent space (2024). Preprint at <https://arxiv.org/abs/2412.06769>.
- [75] McCoy, R. T., Yao, S., Friedman, D., Hardy, M. D. & Griffiths, T. L. Embers of autoregression show how large language models are shaped by the problem

- they are trained to solve. *Proceedings of the National Academy of Sciences* **121**, e2322420121 (2024). URL <https://www.pnas.org/doi/abs/10.1073/pnas.2322420121>.
- [76] Vong, W. K., Wang, W., Orhan, A. E. & Lake, B. M. Grounded language acquisition through the eyes and ears of a single child. *Science* **383**, 504–511 (2024). URL <https://www.science.org/doi/abs/10.1126/science.adi1374>.
- [77] Stolk, A., Verhagen, L. & Toni, I. Conceptual alignment: How brains achieve mutual understanding. *Trends in Cognitive Sciences* **20**, 180–191 (2016). URL <https://www.sciencedirect.com/science/article/pii/S1364661315002867>.
- [78] Collins, K. M. *et al.* Building machines that learn and think with people. *Nature Human Behaviour* **8**, 1851–1863 (2024). URL <https://doi.org/10.1038/s41562-024-01991-9>.
- [79] Dubey, A. *et al.* The Llama 3 Herd of Models (2024). Preprint at <https://arxiv.org/abs/2407.21783>.
- [80] Almazrouei, E. *et al.* The falcon series of open language models (2023). Preprint at <https://arxiv.org/abs/2311.16867>.
- [81] Team, G. *et al.* Gemma 2: Improving open language models at a practical size (2024). Preprint at <https://arxiv.org/abs/2408.00118>.
- [82] Touvron, H. *et al.* Llama: Open and efficient foundation language models (2023). Preprint at <https://arxiv.org/abs/2302.13971>.
- [83] Touvron, H. *et al.* Llama 2: Open foundation and fine-tuned chat models (2023). Preprint at <https://arxiv.org/abs/2307.09288>.
- [84] Jiang, A. Q. *et al.* Mistral 7b (2023). Preprint at <https://arxiv.org/abs/2310.06825>.
- [85] Jiang, A. Q. *et al.* Mixtral of experts (2024). Preprint at <https://arxiv.org/abs/2401.04088>.
- [86] Zhang, G. *et al.* Map-neo: Highly capable and transparent bilingual large language model series (2024). Preprint at <https://arxiv.org/abs/2405.19327>.
- [87] Groeneveld, D. *et al.* Ku, L.-W., Martins, A. & Srikumar, V. (eds) *OLMo: Accelerating the science of language models*. (eds Ku, L.-W., Martins, A. & Srikumar, V.) *Proceedings of the 62nd Annual Meeting of the Association for Computational Linguistics (Volume 1: Long Papers)*, 15789–15809 (Association for Computational Linguistics, Bangkok, Thailand, 2024). URL <https://aclanthology.org/2024.acl-long.841>.

- [88] Zhang, S. *et al.* Opt: Open pre-trained transformer language models (2022). Preprint at <https://arxiv.org/abs/2205.01068>.
- [89] Li, Y. *et al.* Textbooks are all you need ii: phi-1.5 technical report (2023). Preprint at <https://arxiv.org/abs/2309.05463>.
- [90] Biderman, S. *et al.* Krause, A. *et al.* (eds) *Pythia: A suite for analyzing large language models across training and scaling*. (eds Krause, A. *et al.*) *Proceedings of the 40th International Conference on Machine Learning*, Vol. 202 of *Proceedings of Machine Learning Research*, 2397–2430 (PMLR, 2023). URL <https://proceedings.mlr.press/v202/biderman23a.html>.
- [91] Bai, J. *et al.* Qwen technical report (2023). Preprint at <https://arxiv.org/abs/2309.16609>.
- [92] Yang, A. *et al.* Qwen2 technical report (2024). Preprint at <https://arxiv.org/abs/2407.10671>.
- [93] Kuperman, V., Stadthagen-Gonzalez, H. & Brysbaert, M. Age-of-acquisition ratings for 30,000 English words. *Behavior Research Methods* **44**, 978–990 (2012). URL <https://doi.org/10.3758/s13428-012-0210-4>.
- [94] Brysbaert, M., Warriner, A. B. & Kuperman, V. Concreteness ratings for 40 thousand generally known English word lemmas. *Behavior Research Methods* **46**, 904–911 (2014). URL <https://doi.org/10.3758/s13428-013-0403-5>.
- [95] Fellbaum, C. *WordNet: An Electronic Lexical Database* (The MIT Press, 1998). URL <https://doi.org/10.7551/mitpress/7287.001.0001>.
- [96] Xu, N., Zhang, Q., Zhang, M., Qian, P. & Huang, X. On the tip of the tongue: Analyzing conceptual representation in large language models with reverse-dictionary probe (2024). Preprint at <https://arxiv.org/abs/2402.14404>.
- [97] Rothschild, L. The distribution of english dictionary word lengths. *Journal of Statistical Planning and Inference* **14**, 311–322 (1986). URL <https://www.sciencedirect.com/science/article/pii/0378375886901692>.
- [98] Kriegeskorte, N. & Diedrichsen, J. Peeling the onion of brain representations. *Annual Review of Neuroscience* **42**, 407–432 (2019). URL <https://www.annualreviews.org/content/journals/10.1146/annurev-neuro-080317-061906>.
- [99] Zhelezniak, V., Savkov, A., Shen, A. & Hammerla, N. Burstein, J., Doran, C. & Solorio, T. (eds) *Correlation coefficients and semantic textual similarity*. (eds Burstein, J., Doran, C. & Solorio, T.) *Proceedings of the 2019 Conference of the North American Chapter of the Association for Computational Linguistics: Human Language Technologies, Volume 1 (Long and Short Papers)*, 951–962 (Association for Computational Linguistics, Minneapolis, Minnesota, 2019). URL

<https://aclanthology.org/N19-1100>.

- [100] Mikolov, T., Sutskever, I., Chen, K., Corrado, G. S. & Dean, J. Burges, C., Bottou, L., Welling, M., Ghahramani, Z. & Weinberger, K. (eds) *Distributed representations of words and phrases and their compositionality*. (eds Burges, C., Bottou, L., Welling, M., Ghahramani, Z. & Weinberger, K.) *Advances in Neural Information Processing Systems*, Vol. 26, 3111–3119 (Curran Associates, Inc., 2013). URL [https://proceedings.neurips.cc/paper\\_files/paper/2013/file/9aa42b31882ec039965f3c4923ce901b-Paper.pdf](https://proceedings.neurips.cc/paper_files/paper/2013/file/9aa42b31882ec039965f3c4923ce901b-Paper.pdf).
- [101] Kaplan, J. *et al.* Scaling laws for neural language models (2020). Preprint at <https://arxiv.org/abs/2001.08361>.
- [102] Wei, J. *et al.* Emergent Abilities of Large Language Models. *Transactions on Machine Learning Research* (2022). URL <https://openreview.net/forum?id=yzkSU5zdwD>.
- [103] Sorscher, B., Ganguli, S. & Sompolinsky, H. Neural representational geometry underlies few-shot concept learning. *Proceedings of the National Academy of Sciences* **119**, e2200800119 (2022). URL <https://www.pnas.org/doi/abs/10.1073/pnas.2200800119>.
- [104] Contier, O., Baker, C. I. & Hebart, M. N. Distributed representations of behaviour-derived object dimensions in the human visual system. *Nature Human Behaviour* **8**, 2179–2193 (2024). URL <https://doi.org/10.1038/s41562-024-01980-y>.
- [105] Allen, E. J. *et al.* A massive 7T fMRI dataset to bridge cognitive neuroscience and artificial intelligence. *Nature Neuroscience* **25**, 116–126 (2022). URL <https://doi.org/10.1038/s41593-021-00962-x>.
- [106] Roads, B. D. & Love, B. C. Modeling similarity and psychological space. *Annual Review of Psychology* **75**, 215–240 (2024). URL <https://www.annualreviews.org/content/journals/10.1146/annurev-psych-040323-115131>.
- [107] Halawi, G., Dror, G., Gabrilovich, E. & Koren, Y. Large-scale learning of word relatedness with constraints (2012). URL <https://doi.org/10.1145/2339530.2339751>. In Proceedings of the 18th ACM SIGKDD International Conference on Knowledge Discovery and Data Mining, Beijing, China, 1406–1414, 2012.



## SI 1 Supplementary Results

### SI 1.1 Assessing the generality of LLMs’ concept inference capacity

To evaluate the generality of our results, we extended our experiment to a broader range of concepts and descriptions. As shown in Fig. S1a–c, the LLMs exhibited strong adaptability. The best-performing model, LLaMA3-70B, achieved an exact match accuracy of 83.00% ( $\pm 0.67\%$ ) on GPT-generated English descriptions, compared to 89.45% ( $\pm 0.30\%$ ) on the original descriptions in THINGS [42], consistently producing proper terms for the same concepts. Performance was slightly lower on the 21,402 concepts in WordNet, with LLaMA3-70B achieving 71.59% ( $\pm 0.30\%$ ) after 24 demonstrations. These findings suggest that concept inference might be more challenging for abstract or complex concepts beyond the concrete object concepts in THINGS [42], such as “have,” “make,” and “take,” which can be harder to describe precisely. Additionally, we observed a modest decline in performance when varying degrees of word order permutations were applied to the query descriptions. Specifically, the exact match accuracy of LLaMA3-70B dropped to 77.52% ( $\pm 0.22\%$ ) under full permutation. This indicates that while LLMs maintain some robustness to input noise, they are at least sensitive to linguistic structures when combining words into coherent conceptual representations.

Results from additional open-source LLMs further validated the generalizability of our findings. For the THINGS database, the exact match accuracy of LLMs we tested improved progressively as the number of demonstrations increased from 1 to 24 (Fig. S1d). This trend aligns with the observations in Results 2.2, though there was notable variability among models. In general, LLMs with a larger number of parameters demonstrated better performance ( $\rho = 0.915$ ,  $P < 0.0001$ , 95% CI: 0.806–0.963, Fig. S1e).

As in Results 2.2, we conducted the counterfactual analysis on another LLM, LLaMA3-8B, to probe the interrelatedness among concepts within it. Similar to LLaMA3-70B, this model gradually shifted from replicating the proxy symbol in context to generating the correct word for the query concept (Fig. S1f). However, it struggled with misleading demonstrations, exhibiting varying performance across different types of proxy symbols and failing to recover its original performance in the standard generalization setting. Specifically, it performed particularly poorly with symbols that lacked semantic content, such as random capital letters or strings of random characters. This suggests that the capacity to leverage contextual cues from other concepts for inference is emergent, and highlights a critical difference among LLMs in capturing interrelationships among concepts.

### SI 1.2 Uncovering a context-independent structure through alternative metrics

Our findings in Results 2.3 suggest that LLMs’ conceptual representations are converging toward a shared, context-independent conceptual structure. This was demonstrated using representational similarity analysis (RSA) [44], with Spearman’s rank correlation

coefficient as the similarity measure. We further validated this result using two additional metrics. The first, also based on RSA, used cosine similarity as the similarity measure, while the second employed the average parallelism score (PS) [58], which quantifies whether the direction of vector offsets between concepts is maintained across contexts (Methods 4.3). Both metrics revealed a consistent trend, where the alignment between representation spaces gradually increased as the number of contextual demonstrations rose from 1 to 24, with marginal gains beyond this threshold (Fig. S2a,c). The alignment with the space formed based on 120 demonstrations increased from 0.759 ( $\pm 0.036$ ) for cosine-similarity-based RSA and 0.840 ( $\pm 0.022$ ) for PS with one demonstration to 0.962 ( $\pm 0.006$ ) and 0.974 ( $\pm 0.003$ ) after 24 demonstrations. The alignment was strongly correlated with the LLM’s exact match accuracy on concept inference ( $\rho = 0.976$ ,  $P < 0.0001$  95% CI: 0.778–1.0 for cosine-similarity-based RSA and  $\rho = 0.976$ ,  $P < 0.0001$  95% CI: 0.795–1.0 for PS; Fig. S2b,d). These results add to the evidence that LLMs are able to construct a context-independent relational structure, which is reflected in their concept inference capacity. They also highlight that various relationships among conceptual representations are preserved across contexts, readily supporting knowledge generalization.

### SI 1.3 Determining suitable similarity functions for representation spaces

To characterize the relational structure of LLM-derived conceptual representations, a proper similarity function is needed [106]. We employed two similarity measures, including cosine similarity and Spearman’s rank correlation, and assessed whether each reflected meaningful relationships between concepts. The resulting similarity scores were compared to with human similarity ratings from two datasets: SimLex-999 [47] and MTurk-771 [107]. While both datasets provide ratings for concept pairs, SimLex-999 explicitly distinguishing semantic similarity from association or relatedness, whereas MTurk-771 focuses primarily on relatedness. Our results (Fig. S3a–b) show that cosine similarity captures genuine semantic similarity instead of relatedness, yielding a correlation of  $\rho = 0.705$  ( $\pm 0.013$ ) on SimLex-999 for representations derived from 48 demonstrations, while the performance on MTurk-771 was  $\rho = 0.668$  ( $\pm 0.008$ ). In contrast, Spearman’s rank correlation aligns well with both semantic similarity and relatedness, achieving  $\rho = 0.771$  ( $\pm 0.009$ ) on SimLex-999 and  $\rho = 0.755$  ( $\pm 0.005$ ) on MTurk-771. We thus adopted Spearman’s rank correlation as our primary similarity function.

We also conducted the same experiments on static word embeddings to determine the appropriate similarity function. The word embeddings achieved high correlation on MTurk-771 ( $\rho = 0.753$  for cosine similarity and  $\rho = 0.745$  for Spearman’s rank correlation), but struggled on SimLex-999 ( $\rho = 0.464$  for cosine similarity and  $\rho = 0.459$  for Spearman’s rank correlation) (Fig. S3a–b). These results indicate that static embeddings primarily reflect relatedness but fail to capture genuine similarity. This aligns with previous research [47] and highlights the distinction between the contextually formed conceptual representations of LLMs and static word embeddings corresponding to word forms. Notably, unlike LLMs, both similarity measures produced comparable

results across the two datasets, with cosine similarity consistently outperforming Spearman’s rank correlation. We therefore used cosine similarity as the similarity function for subsequent analysis.

#### **SI 1.4 Evaluating different approaches to similarity-based categorization**

To investigate whether LLMs’ conceptual representations support similarity-based categorization, we applied three distinct strategies grounded in different theories of concepts: the prototype, exemplar, and relational views. Our results (Fig. S3c) reveal that LLM-derived conceptual representations generally enable accurate categorization, with the prototype-based approach yielding the best performance ( $92.25\% \pm 0.15\%$  with 48 demonstrations), followed by the exemplar-based approach ( $88.49\% \pm 0.18\%$ ). By comparison, categorization based on relationships between categories and individual concepts requires more contextual demonstrations, reaching  $82.10\%$  ( $\pm 1.24\%$ ) after 48 demonstrations. This suggests that the representations for categories bear meaningful relationships with associated concepts, though sufficient demonstrations are needed to form effective relational structures. LLM-derived conceptual representations, still, significantly outperformed static word embeddings across all three strategies, which underscores their capacity to form coherent structures that align closely with human knowledge.

#### **SI 1.5 Recovering context-dependent knowledge from LLM conceptual representations without extreme feature values**

Our results (Results 2.4) suggest that LLM-derived conceptual representations can effectively recover context-dependent human ratings across categories and features. However, to simulate appropriate context, we presented LLMs with two demonstrations for each category-feature pair, which showcases the extreme values of the target feature within that category. This might raise concerns about whether the alignment with human ratings is influenced by these outliers. While this should not be the case, as Spearman’s rank correlation is robust to these values, we further validated our findings by reanalyzing all category-feature pairs after removing the two items with the most extreme values used in the demonstrations. The results are presented in Fig. S4, demonstrating high correlations with human ratings for the majority of category-feature pairs (47 out of 52;  $\rho > 0.5$ ,  $P < 0.001$ , FDR corrected). The median correlation slightly decreased from 0.817 to 0.795, while the split-half reliability of human ratings also reduced marginally from 0.954 to 0.946. Meanwhile, LLM-derived conceptual representations consistently outperformed static word embeddings across most category-feature pairs (Fig. S5). These findings reaffirm the effectiveness of LLM conceptual representations in handling context-dependent computations of human knowledge.

## SI 1.6 Exploring advantages and limitations of LLM conceptual representations in explaining brain activity patterns

To rigorously test the effectiveness of LLM-derived conceptual representations in elucidating the neural coding of concepts, we compared them against two baseline representations including the 300-dimensional fastText word embedding and a 66-dimensional embedding [40] trained on and validated to successfully account for human similarity judgments for the THINGS concepts. We used variance partitioning for each baseline representation to disentangle their unique contributions in explaining neural activity. To conservatively estimate the unique variance explained by LLM-derived representations, we reduced their dimensionality to match that of the baseline representation. Fig. S7 and Fig. S8 present the results for all three participants, which are consistent with Results 2.5.

For comparison, we conducted additional experiments preserving each representation’s original dimensionality. The results generally align with those obtained with dimensionality-reduced LLM conceptual representations (Fig. S9 and Fig. S10), with the LLM conceptual representations alone explaining a larger portion of the variance across the visual cortex and beyond. However, some information, primarily within the low-level visual cortex, remains uniquely captured by the similarity embedding, indicating that certain aspects of behaviorally relevant visual information are not fully captured by LLMs.

To explore these unexplained aspects, we regressed the similarity embedding onto the LLM-derived conceptual representations (Methods SI 2.3). The dimensions of the similarity embedding were sparse, non-negative, and ordered by their weights in representing object concepts. As illustrated in Fig. S11, dimensions with higher weights were generally better explained by LLM representations, which effectively captured higher-level properties such as taxonomic membership (e.g., “animal-related” and “food-related”) and function (e.g., “transportation-/movement-related”). In contrast, perceptual properties such as color (e.g., “orange,” “yellow,” “red” and “black”), texture (e.g. “fine-grained pattern”) and shape (e.g., “cylindrical/conical/cushioning”) were poorly accounted for, with color being the most inadequately represented. This highlights a potential limitation of LLM conceptual representations, learned solely from language, in capturing visually grounded information. Incorporating grounded information thus offers a promising direction for enhancing alignment with human concepts [65, 76].

## SI 2 Supplementary Methods

### SI 2.1 Description generation using ChatGPT

We used the following template to prompt GPT-3.5 (gpt-3.5-turbo-0125) to generate descriptions for the concepts in THINGS: “Provide three distinct definitions of the word ‘[Word]’ (referring to ‘[Description]’) that vary in linguistic forms, without explicitly including the word itself. Try to be concise.”

## SI 2.2 Exemplar-based categorization

We implemented exemplar-based categorization using a nearest-neighbour decision rule [103], where a test example  $\mathbf{x}_t$  was compared to all other examples  $\mathbf{x}_e$  and categorized based on their relative similarities. Formally, the distance between the test example and each exemplar was computed as

$$d(\mathbf{x}_t, \mathbf{x}_e) = 1 - \text{similarity}(\mathbf{x}_t, \mathbf{x}_e). \quad (\text{S1})$$

The support for each category  $K$  was then calculated as

$$\text{Support}(K) = \frac{1}{|K|} \sum_{\mathbf{x}_e \in K} \exp(-\beta \cdot d(\mathbf{x}_t, \mathbf{x}_e)), \quad (\text{S2})$$

where  $|K|$  denotes the number of examples in class  $K$ , and  $\beta$  is a hyperparameter that controls the weighting of distances. The test example was assigned to the category with the highest support. After testing a range of  $\beta$  values ranging from  $10^{-6}$  to  $10^4$ , we set  $\beta = 100$ , as it consistently produced the best results.

## SI 2.3 Regression model for similarity embedding

To analyze the information missing from LLM-derived conceptual representations, we regressed the embedding learned from human similarity judgments [40] onto these representations through a linear ridge regression model. This also served as an intermediate step in variance partitioning (Methods 4.10). The similarity embedding consisted of 66 dimensions for each of the 1,854 concepts in THINGS. As in Methods 4.9, we modeled the value of each dimension as  $y_{d,c} = \mathbf{h}_c \mathbf{w} + b + \epsilon$ , where  $y_{d,c}$  is the value at dimension  $d$  for concept  $c$ ,  $\mathbf{h}_c$  is the corresponding LLM representation,  $\mathbf{w}$  is a vector of regression weights,  $b$  is a constant, and  $\epsilon$  denotes residual error. Model performance was assessed through twenty-fold cross-validation with non-overlapping concepts, evaluating the  $R^2$  between predicted and observed values across folds.

## SI 3 Supplementary Figures and Tables

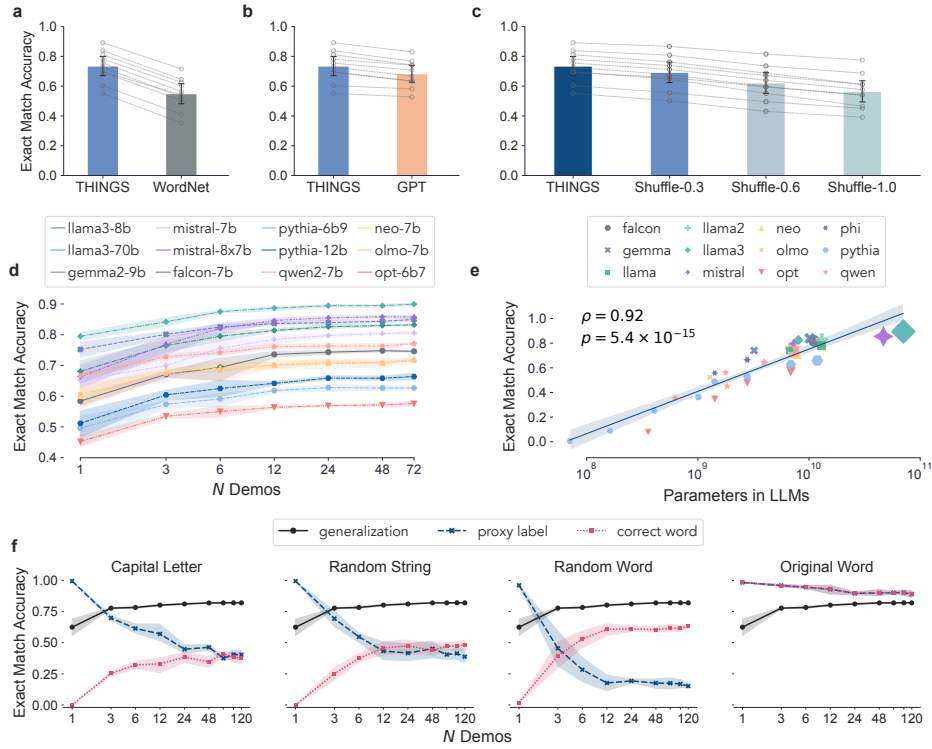


**Fig. S1** LLMs can generalize to a broader range of concepts and descriptions. **a–c**, Performance of LLMs on different sets of descriptions and concepts, compared to their performance on THINGS given 24 demonstrations. LLMs that excel on THINGS also adapt more effectively to diverse descriptions and concepts. **a**, Performance on concepts spanning different word classes, degrees of concreteness, and age-of-acquisition, sourced from WordNet. **b**, Performance on descriptions of the same concepts in THINGS, generated by GPT-3.5. **c**, Performance on descriptions of concepts in THINGS under increasing degree of word order permutations. Error bars represent 95% confidence intervals, calculated from the average performance across five independent runs of different models. **d**, Performance of various LLMs on the reverse dictionary task, evaluated on the THINGS database and measured through exact match accuracy. The models were presented with  $N$  demonstrations sampled from the training set and evaluated on an independent test set. Shaded areas denote 95% confidence intervals, calculated from 10,000 resamples across five independent runs. **e**, Larger LLMs tend to perform better on concept inference. Each point represents an LLM, plotted in proportion to its scale and color-coded by model series. The x-axis denotes the number of parameters, and the y-axis shows the model’s performance on the reverse dictionary task, given 24 demonstrations and averaged across five runs. **f**, LLaMA3-8B struggles more with misleading demonstrations compared to LLaMA3-70B, though still sensitive to relationships among concepts. The black line denotes the model’s performance when presented with  $N$  demonstrations in the standard setting. The blue and red lines illustrate the model’s behavior when given one misleading demonstration—a description paired with a proxy label (as indicated in the figure titles)—and  $N - 1$  correct demonstrations of other concepts. The blue line shows the frequency with which the model copies the proxy label, while the red line indicates how often it generates the correct word for the query concept based on contextual information from other concepts. Shaded areas represent 95% bootstrapped confidence intervals, calculated from 10,000 resamples over five independent runs.

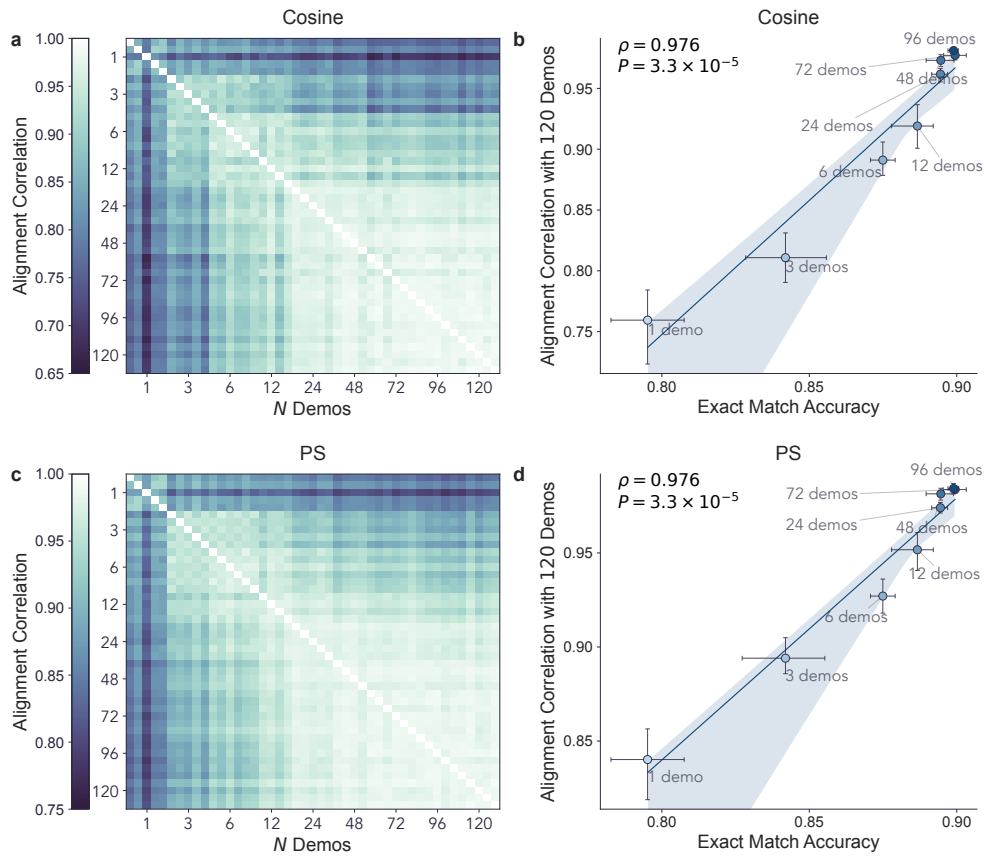


**Fig. S2** LLMs converge toward a context-independent representational structure of concepts. **a,c**, Alignment correlation between the LLM-derived conceptual representations across different contextual demonstrations, measured through cosine-similarity-based RSA (**a**) and PS (**c**), respectively. The LLM (LLaMA3-70B) was presented with  $N$  randomly selected demonstrations, repeated across five independent runs. **b,d**, LLM performance on the reverse dictionary task reflects alignment with the representations formed from 120 demonstrations, measured through cosine-similarity-based RSA (**b**) and PS (**d**), respectively. Each point corresponds to the representations formed by the LLM based on  $N$  demonstrations, with the x-axis showing performance and the y-axis indicating alignment correlation. Error bars denote 95% confidence intervals, calculated from 10,000 bootstrap resamples across five independent runs.

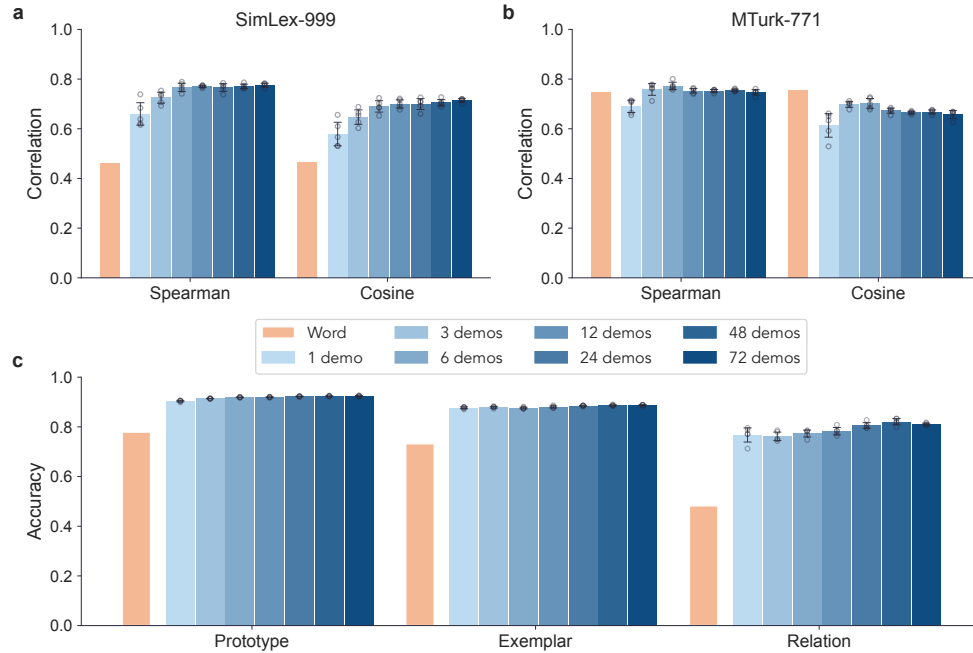


**Fig. S3** LLM-derived conceptual representations support the computation of similarity, relatedness and categorization. **a–b**, Evaluation of alignment between LLM-derived conceptual representations and psychological measures of similarity using two different similarity measures including Spearman’s rank correlation and cosine similarity. **a**, Correlation of LLM-derived representations with human similarity ratings from SimLex-999, which focuses on genuine semantic similarity. **b**, Correlation with human similarity ratings from MTurk-771, which measures relatedness. LLM-derived conceptual representations significantly outperform static word embeddings on semantic similarity, with word embeddings primarily reflecting relatedness. **c**, Performance of LLM-derived conceptual representations in similarity-based categorization, showing a significant improvement over static word embeddings. Each plot displays the accuracy of these representations for a distinct categorization strategy: prototype-based, exemplar-based, or relation-based. Error bars represent 95% confidence intervals computed from five independent runs.



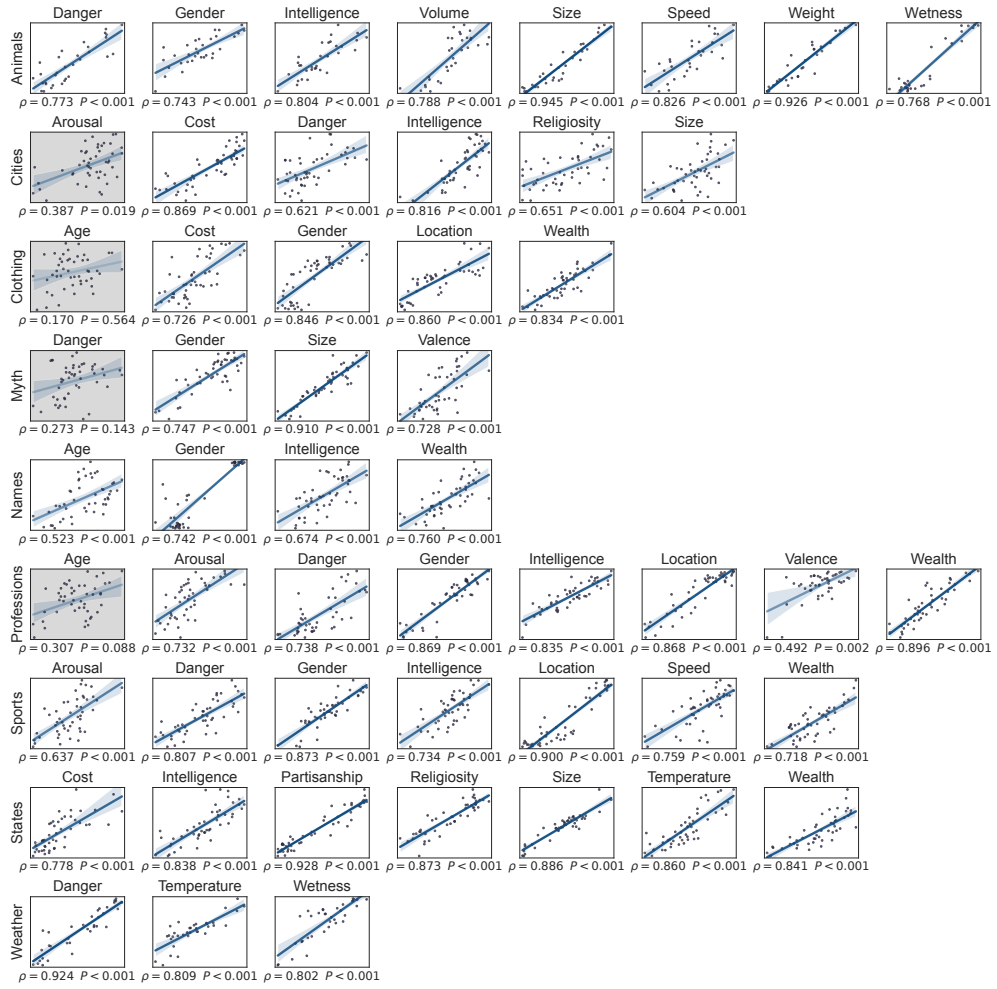


**Fig. S4** Performance of conceptual representations derived from LLaMA3-70B in predicting context-dependent human judgments across 52 category-feature pairs, with the most extreme values excluded. Scatter plots illustrate the relationship between predicted ratings from conceptual representations (x-axis) and the average human ratings (y-axis). Linear fits are shown as straight lines, with shaded regions representing 95% confidence intervals derived from 10,000 bootstrap resamples. Category-feature pairs with statistically significant correlations (Spearman's rank correlation, FDR  $P < 0.01$ ) are displayed against a white background.

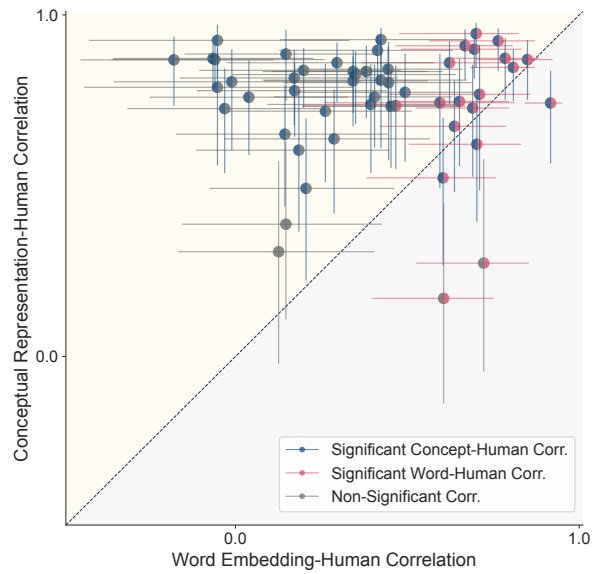


**Fig. S5** Comparison of LLM-derived conceptual representations and static word embeddings in predicting context-dependent human ratings, with the most extreme values excluded. The x-axis represents correlations with human ratings based on static word embeddings, while the y-axis represents correlations based on conceptual representations derived from LLaMA3-70B. Colored points indicate significant correlations (Spearman’s rank correlation, FDR  $P < 0.01$ ). Error bars represent 95% confidence intervals estimated from 10,000 bootstrap resamples.

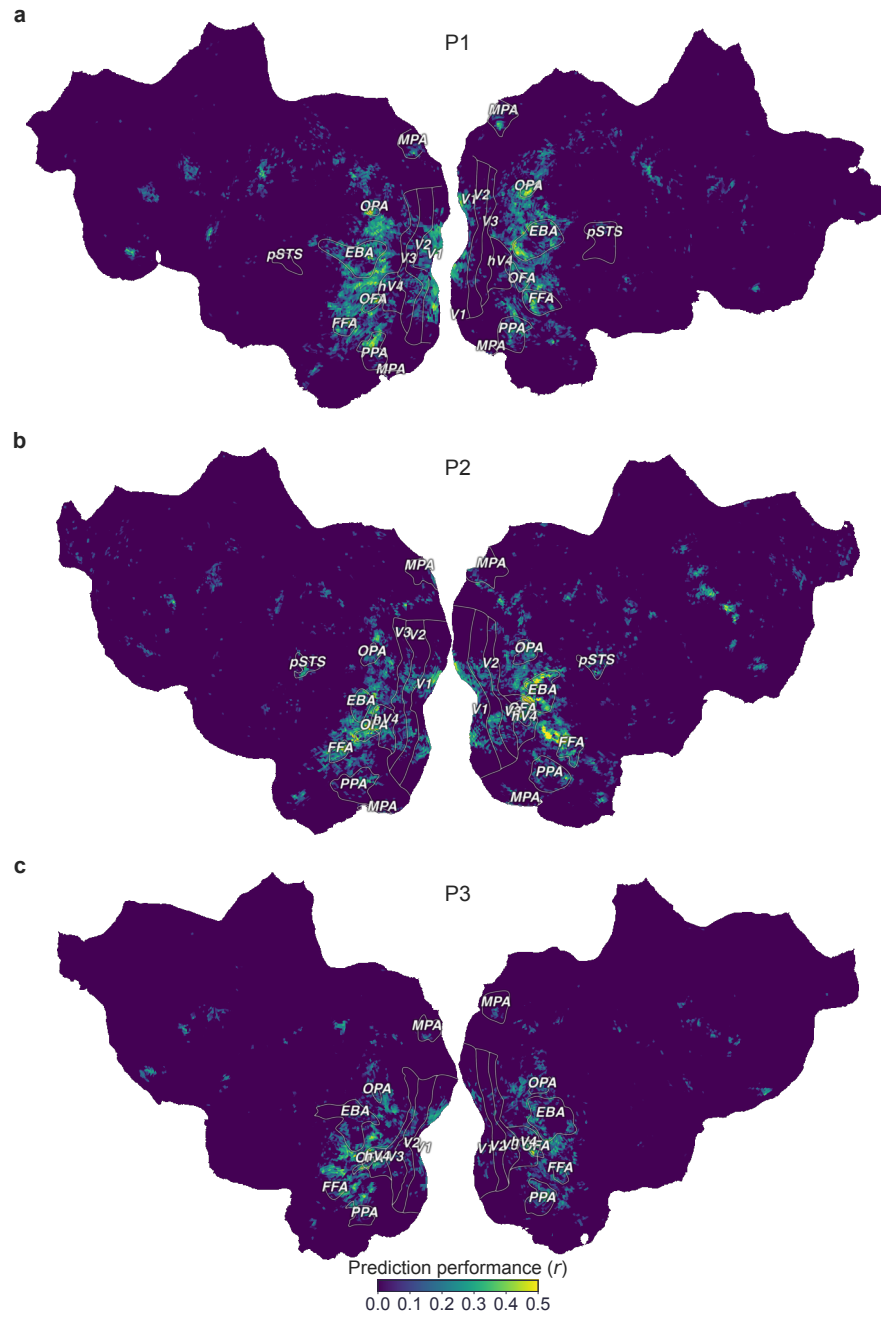


**Fig. S6** fMRI prediction performance of LLM-derived conceptual representations (LLaMA3-70B) assessed via Pearson's correlation ( $r$ ). **a-c** show the cortical maps of prediction performance for three individual participants. Only voxels with statistically significant correlations between predicted and observed brain activations are color-coded ( $P < 0.01$ , FDR corrected).

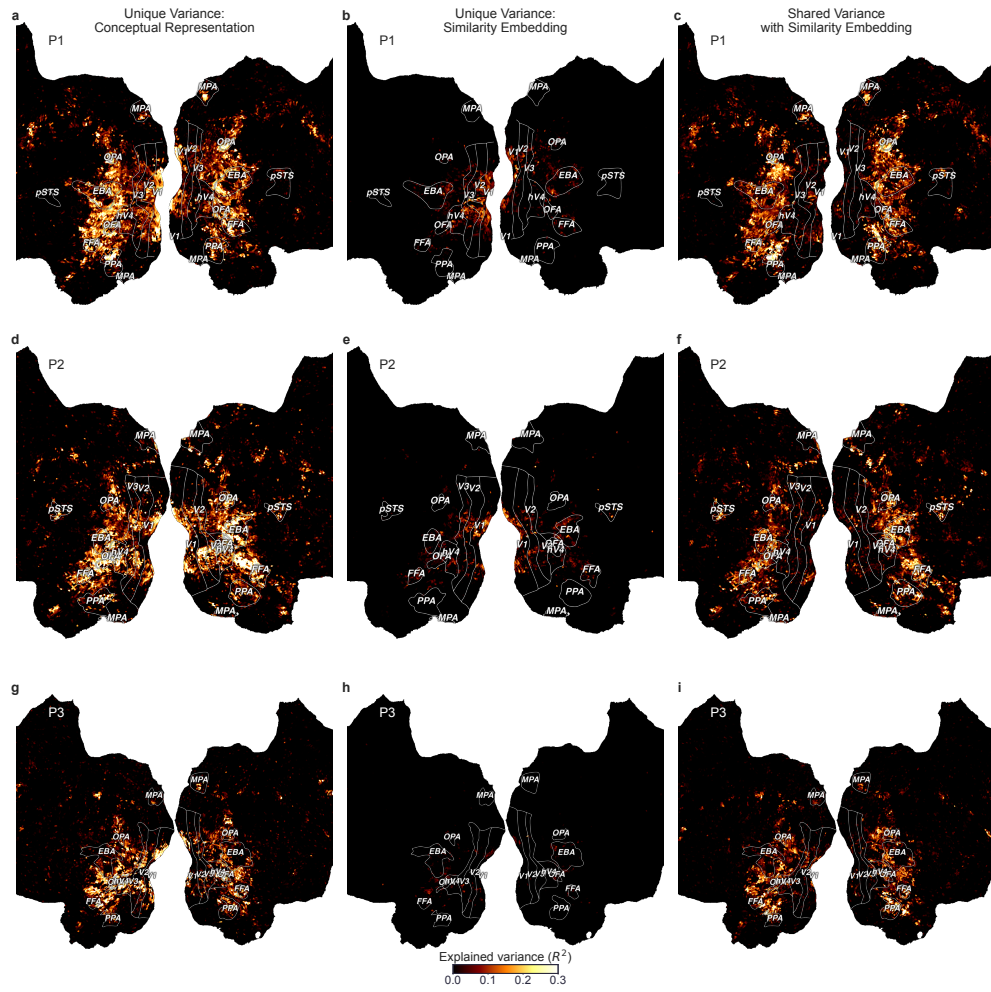


**Fig. S7** Comparison between LLM-derived conceptual representation and a similarity embedding learned from human similarity judgments, with LLM-derived conceptual representations reduced to 66 dimensions to match the dimensionality of the similarity embedding. **a**, Variance uniquely explained by the LLM-derived conceptual representation. **b**, Variance uniquely explained by the similarity embedding. **c**, Shared variance explained by both models. **a–c**, **d–f**, and **g–i** show results for each of the three participants, respectively. The colors represent the proportion of explained variance, normalized relative to the noise ceiling and averaged over five runs.

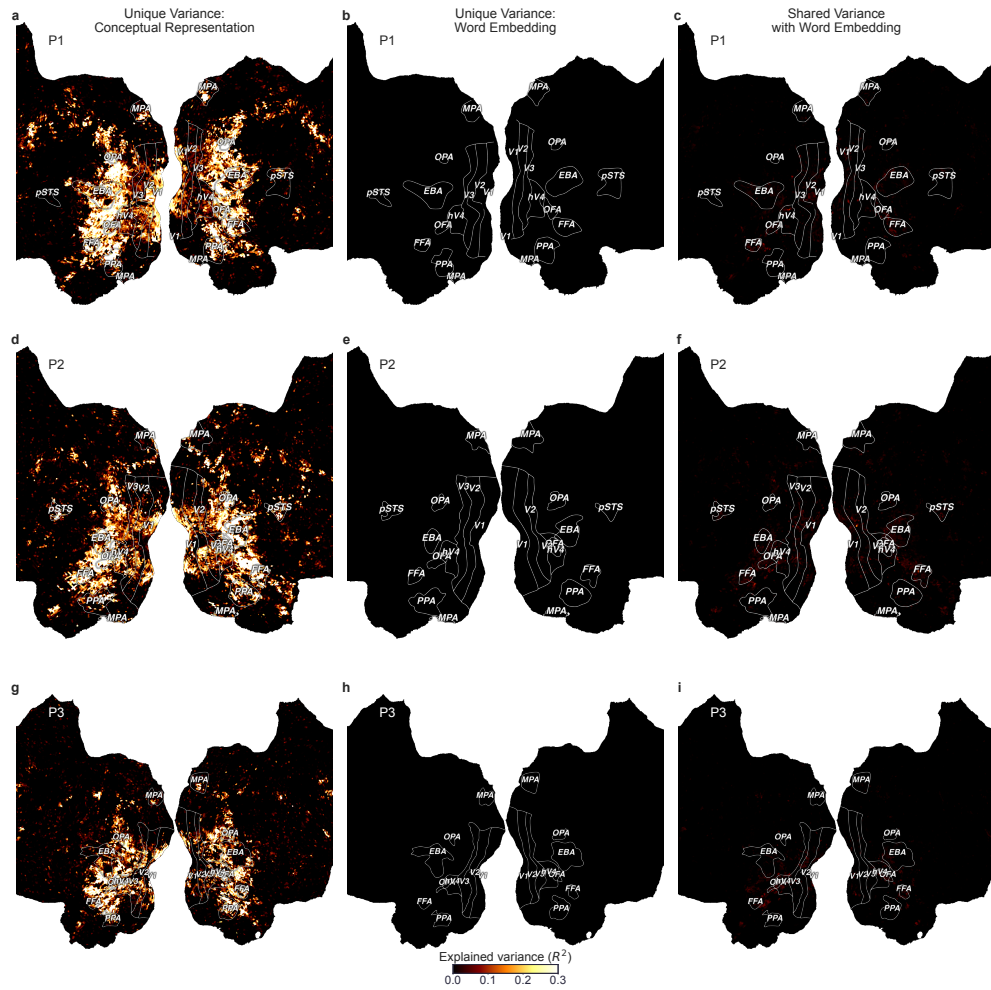


**Fig. S8** Comparison between LLM-derived conceptual representation and a static word embedding (fastText), with LLM-derived conceptual representations reduced to 300 dimensions to match the word embedding dimensionality. **a**, Variance uniquely explained by the LLM-derived conceptual representation. **b**, Variance uniquely explained by the static word embedding. **c**, Shared variance explained by both models. **a–c**, **d–f**, and **g–i** show results for each of the three participants, respectively. The colors represent the proportion of explained variance, normalized relative to the noise ceiling and averaged over five runs.

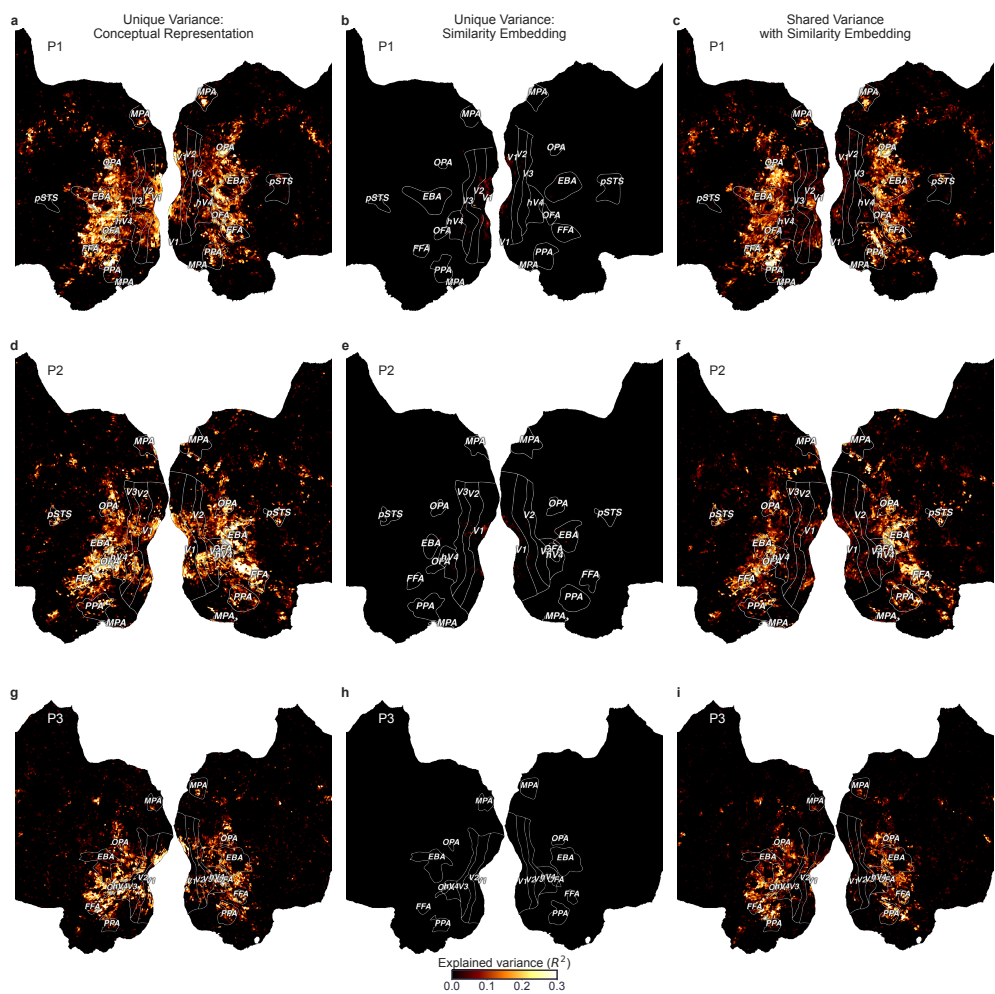


**Fig. S9** Comparison between LLM-derived conceptual representations and a similarity embedding learned from human similarity judgments, with both representations preserved in their original dimensionality. **a**, Variance uniquely explained by the LLM-derived conceptual representation. **b**, Variance uniquely explained by the similarity embedding. **c**, Shared variance explained by both models. **a–c**, **d–f**, and **g–i** show results for each of the three participants, respectively. The colors represent the proportion of explained variance, normalized relative to the noise ceiling and averaged over five runs.

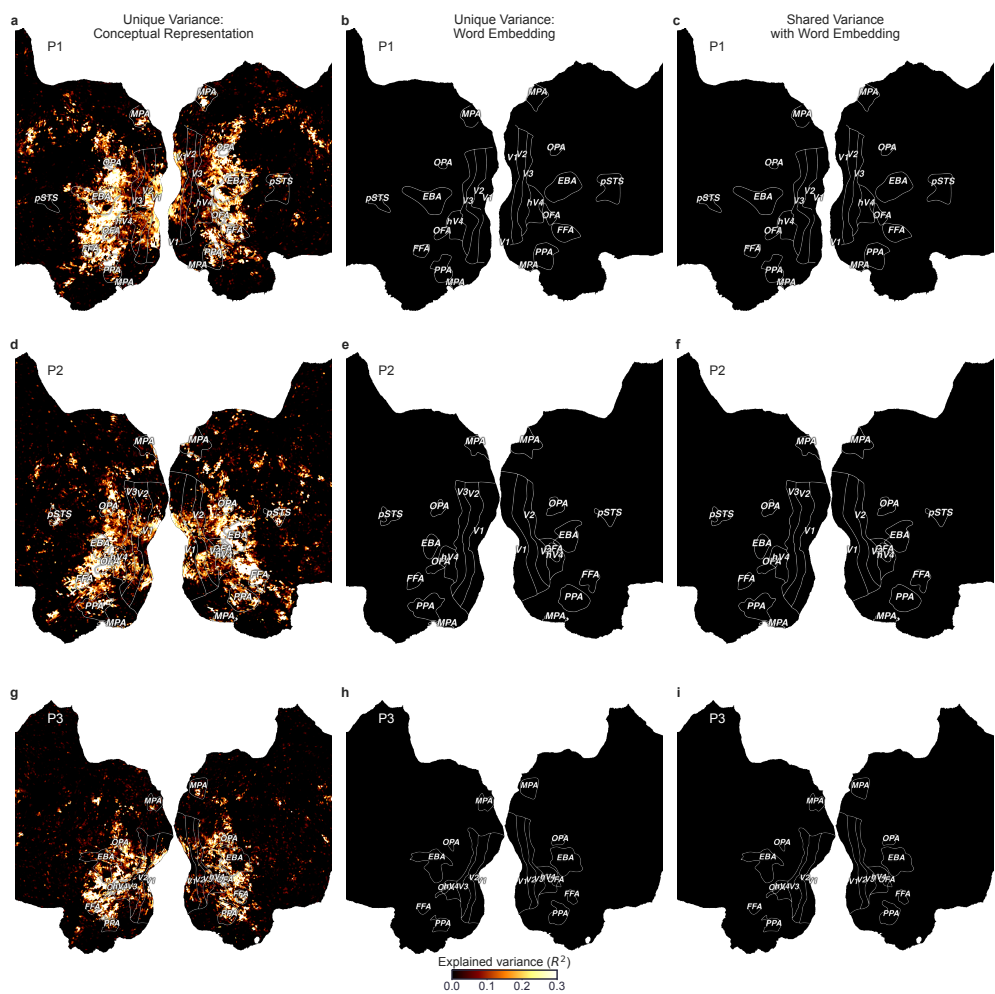


**Fig. S10** Comparison between LLM-derived conceptual representation and a static word embedding (fastText), with both representations preserved in their original dimensionality. **a**, Variance uniquely explained by the LLM-derived conceptual representation. **b**, Variance uniquely explained by the static word embedding. **c**, Shared variance explained by both models. **a–c**, **d–f**, and **g–i** show results for each of the three participants, respectively. The colors represent the proportion of explained variance, normalized relative to the noise ceiling and averaged over five runs.

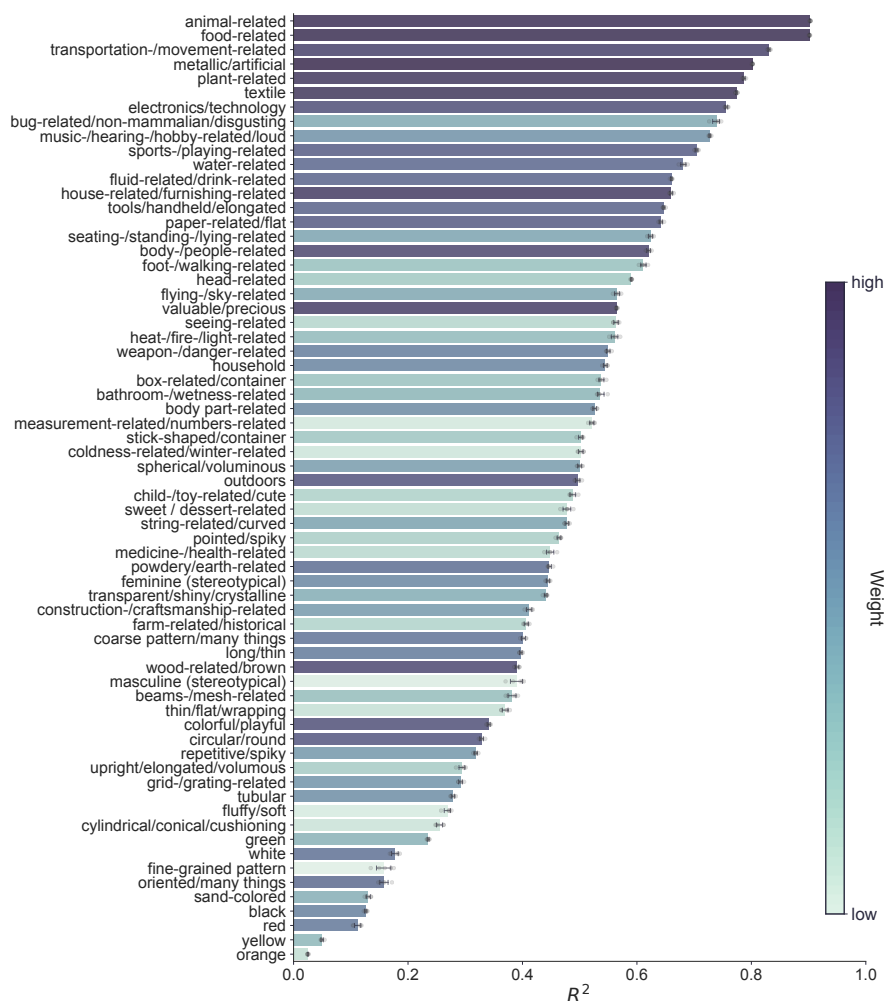


**Fig. S11** Dimensions of an embedding of human similarity judgments as explained by LLM-derived conceptual representations, measured by  $R^2$ . Each bar corresponds to one dimension of the similarity embedding, with its interpretation provided by human annotators. Bars are color-coded based on the relative weight of each dimension. Error bars represent 95% confidence intervals, calculated from five independent runs.



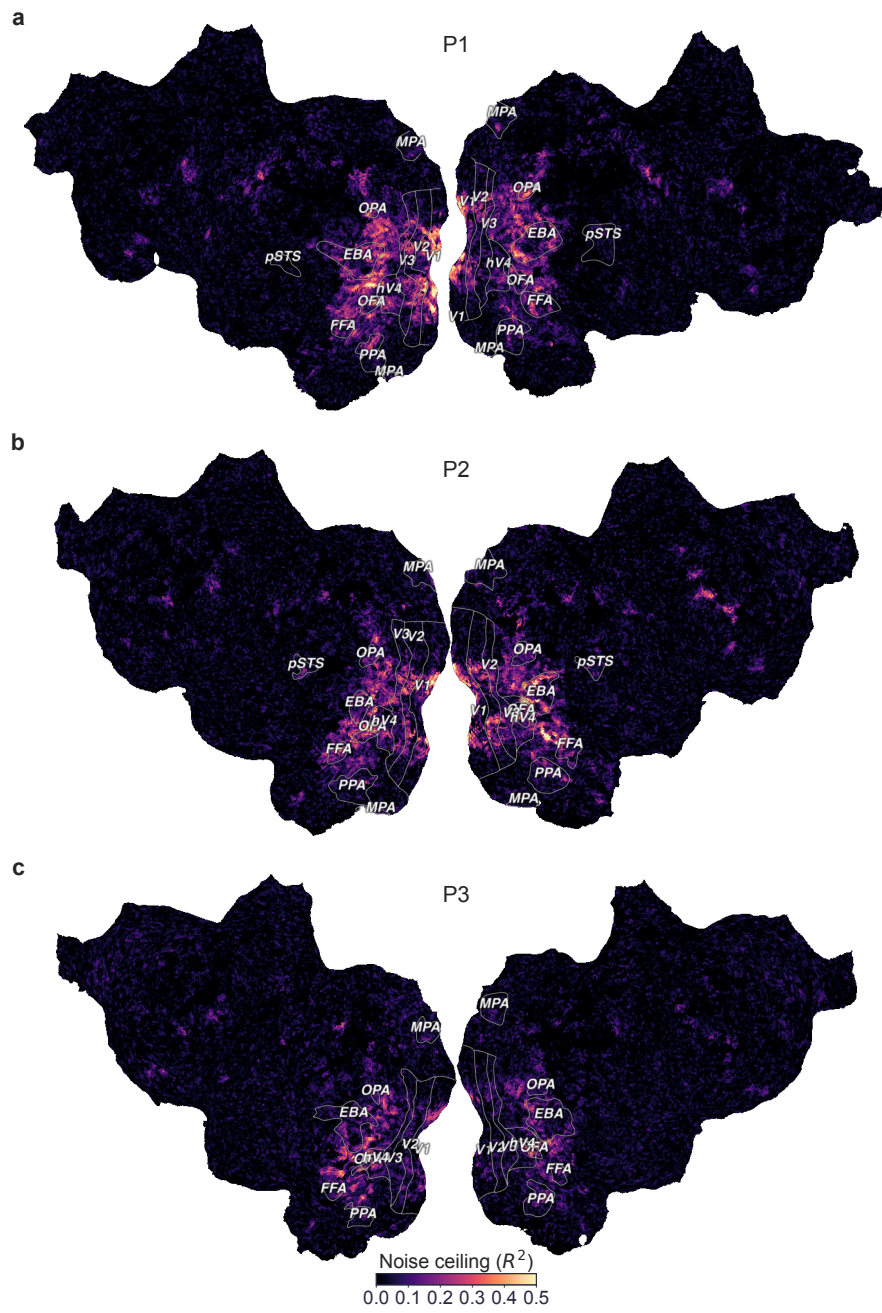


**Fig. S12** Noise ceilings estimated for brain responses of three participants. Colors represent the explainable variance ( $R^2$ ) in neural responses for different concepts. These noise ceilings were used to normalize the prediction performance across concepts.

**Table S1** Major LLMs used in our experiments. The columns “#Parameters” and “#Tokens” represent each model’s scale (number of parameters) and training data volume (number of tokens), respectively. For Mistral models, as the training data volume is not publicly available, we estimated it based on the training data of LLaMA 2 models, which were used for comparison in the Mistral paper [84, 85]. All LLMs are available at <https://huggingface.co>.

Series	Model	#Parameters	#Tokens
Falcon	<a href="#">tiiuae/falcon-7b</a>	7.2B	1.5T
Gemma	<a href="#">google/gemma-2-2b</a>	3.2B	2T
	<a href="#">google/gemma-2-9b</a>	10.2B	8T
LLaMA 1	<a href="#">huggyllama/llama-7b</a>	6.7B	1T
	<a href="#">huggyllama/llama-13b</a>	13.0B	
LLaMA 2	<a href="#">meta-llama/Llama-2-7b</a>	6.7B	2T
	<a href="#">meta-llama/Llama-2-13b</a>	13.0B	
LLaMA 3	<a href="#">meta-llama/Meta-Llama-3-8B</a>	8.0B	15T+
	<a href="#">meta-llama/Meta-Llama-3-70B</a>	70.6B	
Mistral	<a href="#">mistralai/Mistral-7B-v0.3</a>	7.2B	2T*
	<a href="#">mistralai/Mixtral-8x7B-v0.1</a>	46.7B	
MAP-Neo	<a href="#">m-a-p/neo_7b</a>	7.8B	4.5T
OLMo	<a href="#">allenai/OLMo-1B-hf</a>	1.3B	3T
	<a href="#">allenai/OLMo-1.7-7B-hf</a>	6.9B	2.5T
OPT	<a href="#">facebook/opt-350m</a>	356.9M	
	<a href="#">facebook/opt-1.3b</a>	1.4B	180B
	<a href="#">facebook/opt-2.7b</a>	2.8B	
	<a href="#">facebook/opt-6.7b</a>	6.9B	
Phi	<a href="#">microsoft/phi-1_5</a>	1.4B	30B
	<a href="#">microsoft/phi-2</a>	2.8B	1.4T
Pythia	<a href="#">EleutherAI/pythia-70m-deduped</a>	70.4M	
	<a href="#">EleutherAI/pythia-160m-deduped</a>	162.3M	
	<a href="#">EleutherAI/pythia-410m-deduped</a>	405.3M	
	<a href="#">EleutherAI/pythia-1b-deduped</a>	1.0B	300B
	<a href="#">EleutherAI/pythia-1.4b-deduped</a>	1.4B	
	<a href="#">EleutherAI/pythia-2.8b-deduped</a>	2.8B	
	<a href="#">EleutherAI/pythia-6.9b-deduped</a>	6.9B	
<a href="#">EleutherAI/pythia-12b-deduped</a>	11.8B		
Qwen	<a href="#">Qwen/Qwen1.5-0.5B</a>	619.6M	3T
	<a href="#">Qwen/Qwen1.5-1.8B</a>	1.8B	3T
	<a href="#">Qwen/Qwen1.5-4B</a>	4.0B	3T
	<a href="#">Qwen/Qwen1.5-7B</a>	7.7B	3T
	<a href="#">Qwen/Qwen2-0.5B</a>	630.2M	12T
	<a href="#">Qwen/Qwen2-1.5B</a>	1.8B	7T
	<a href="#">Qwen/Qwen2-7B</a>	7.6B	7T

**Table S2** Additional checkpoints of LLMs utilized in our experiments.

Series	Model	#Parameters	#Tokens
MAP-Neo	m-a-p/neo_7b/20.97B	7.8B	20.97B
	m-a-p/neo_7b/41.94B		41.94B
	m-a-p/neo_7b/83.89B		83.89B
	m-a-p/neo_7b/157.29B		157.29B
	m-a-p/neo_7b/251.66B		251.66B
	m-a-p/neo_7b/387.97B		387.97B
	m-a-p/neo_7b/524.29B		524.29B
	m-a-p/neo_7b/681.57B		681.57B
	m-a-p/neo_7b/723.52B		723.52B
OLMo	allenai/OLMo-1.7-7B-hf-step1000	6.9B	4B
	allenai/OLMo-1.7-7B-hf-step5000		20B
	allenai/OLMo-1.7-7B-hf-step10000		41B
	allenai/OLMo-1.7-7B-hf-step15000		62B
	allenai/OLMo-1.7-7B-hf-step20000		83B
	allenai/OLMo-1.7-7B-hf-step36000		150B
	allenai/OLMo-1.7-7B-hf-step72000		301B
	allenai/OLMo-1.7-7B-hf-step126000		528B
	allenai/OLMo-1.7-7B-hf-step197000		825B
	allenai/OLMo-1.7-7B-hf-step240000		1006B
	allenai/OLMo-1.7-7B-hf-step287000		1203B
	allenai/OLMo-1.7-7B-hf-step334000		1400B
	allenai/OLMo-1.7-7B-hf-step382000		1601B
	allenai/OLMo-1.7-7B-hf-step430000		1802B
Pythia	EleutherAI/pythia-6.9b-deduped-step256	6.9B	0.5B
	EleutherAI/pythia-6.9b-deduped-step512		1.1B
	EleutherAI/pythia-6.9b-deduped-step1000		2.1B
	EleutherAI/pythia-6.9b-deduped-step2000		4.2B
	EleutherAI/pythia-6.9b-deduped-step4000		8.4B
	EleutherAI/pythia-6.9b-deduped-step8000		16.8B
	EleutherAI/pythia-6.9b-deduped-step16000		33.6B
	EleutherAI/pythia-6.9b-deduped-step24000		50.3B
	EleutherAI/pythia-6.9b-deduped-step32000		67.1B
	EleutherAI/pythia-6.9b-deduped-step48000		100.7B
	EleutherAI/pythia-6.9b-deduped-step64000		134.2B
	EleutherAI/pythia-6.9b-deduped-step96000		201.3B
	EleutherAI/pythia-6.9b-deduped-step128000		268.4B